CALIFORNIA INSTITUTE OF TECHNOLOGY

SM Report 88-6

Contract N00014-85-K-0596

THREE DIMENSIONAL EFFECTS NEAR A CRACK TIP IN A DUCTILE THREE POINT BEND SPECIMEN - PART I: A NUMERICAL INVESTIGATION

by

R. Narasimhan* and A.J. Rosakis**

Division of Engineering and Applied Science
California Institute of Technology
Pasadena, CA 91125 U.S.A.

January 1988

* Present Affiliation: Assistant Professor, Department of Mechanical Engineeing, Indian Institute of Technology, Powai, Bombay 40076, INDIA.

** Associate Professor of Aeronautics and Applied Mechanics, Division of Engineering and Applied Science, California Institute of Technology, Pasadena, California 91125, Associate Member of ASME.

ABSTRACT

A simultaneous numerical and experimental investigation is undertaken to assess three dimensional effects and HRR dominance near a crack front in a ductile 3-point bend specimen. In parallel to the 3-D numerical calculations, a plane strain and a plane stress analysis of the same in-plane specimen geometry is performed to obtain upper and lower bounds for the 3-D calculation. The radial, angular and thickness variation of the stresses and displacements are studied in great detail from contained yielding, to fully plastic conditions. The results indicate that the plane strain HRR field prevails in the interior of the specimen very near the crack front even for moderate extents of yielding. On the other hand, for distances from the crack tip exceeding about half a specimen thickness, plane stress conditions are approached.

The calculations presented here model a series of laboratory experiments involving three independent experimental techniques. Details regarding the experiments and comparisons of the experimental measurements with numercial calculations and theory are emphasized in Part II of this work.

1. INTRODUCTION

Fracture in structural components of practical dimensions which are made of low-to-intermediate strength metals is often accompanied by extensive plastic deformation prior to crack initiation. Hence, one is compelled to seek elastic-plastic solutions to crack problems to treat such situations. The HRR solution, (Hutchinson, 1968, and Rice, 1968) describes the asymptotic stress and strain variations near a monotomically loaded stationary crack tip in a material characterized by the deformation plasticity theory under two dimensional (plane strain, or plane stress or anti-plane shear) conditions. The J integral (Rice, 1968) which may be interpreted as the energy release rate for a material obeying the deformation plasticity theory also provides a measure of the intensity of the near-tip fields in the HRR solution.

As emphasized by Hutchinson (1983), it is imperative that the HRR solution should dominate over a size scale which is large as compared with the region near the tip wherein finite strain effects are important. The above requirement ensures that J can be safely used to

characterize the initiation of crack growth in ductile materials.

It has recently been demonstrated, on the basis of plane-strain calculations, that finite strain effects become important only for distances from the tip of the order of 2 or 3 times the crack tip opening displacement.

The issue of J-dominance has been examined by many investigators in a variety of situations, ranging from contained yielding to fully plastic conditions under Mode I plane strain (Shih and German, 1981 and McMeeking and Parks, 1979). As an outcome of these studies, it has become possible to specify proper dimensions for some commonly used specimens in fracture toughness testing, so that J-dominance could be ensured. As noted by Hutchinson (1983), analogous specifications for plane stress have not as yet been obtained. Nevertheless, the issue of HRR dominance has partly been addressed by Narasimhan and Rosakis (1988), by means of a detailed, numerical calculation which modeled Mode I, plane stress cracks under small scale yield conditions.

All the analyses mentioned in the foregoing section are based on the assumption of two dimensional plane strain or plane stress conditions. No analytical asymptotic solution exists near three dimensional crack fronts in elastic-plastic materials. In view of the above, it is important to examine the regions near the crack front in which the plane stress and plane strain HRR solutions provide a good approximation to the actual three-dimensional fields. It is generally assumed (see for example Li, Shih, and Needleman, 1985) that plane strain conditions prevail as the crack front is approached, at least in the interior of the specimen. But it appears that no detailed investigation of the region of dominance of any singular elastic-plastic field has been carried out under three-dimensional conditions. This issue is pivotal to the definition of a local energy release rate (pointwise along the crack front), see for example (Li, Shih and Needleman, 1985, and Nakamura, Shih and Freund, 1986a, and 1986b). and its interpretation as an amplitude factor of the near-tip fields.

Surface integral generalizations of the line integral expression of J to three-dimensional crack problems are available in the literature (see for example Budiansky and Rice, 1973). Nevertheless, the definition of a local (pointwise) energy release rate and its numerical computation has been the subject of much investigation (Li, Shih and Needleman, 1985, Shih, Moran and Nakamura, 1986, Nakamura, Shih and Freund, 1986a, Delorenzi and Shih, 1983, Wellman,

Rolfe, and Dodds, 1987, and Dodds, Carpenter and Sorem, 1987).

In Delorenzi and Shih, (1983), Wellman, Rolfe and Dodds (1987), Dodds, Carpenter and Sorem (1987), and Nicholas and Luxmoore (1987), fracture parameters such as J and crack opening displacement are computed using three dimensional numerical solutions for compact tension and three point bend specimens and are compared with experimental results. The variation of three fracture parameters and of the stresses through the thickness are also examined in Delorenzi and Shih, (1983) Wellman, Rolfe and Dodds (1987), Dodds, Carpenter and Sorem, (1987), and Nicholas and Luxmoore (1987).

The purpose of the present investigation is twofold. Firstly, numerical and experimental methods are simultaneously used to assess the effects of three dimensionality near a crack front in a ductile three point bend specimen. The experiments are based on the optical methods of caustics and interferometry and are described in detail in Part II of this investigation. (Zehnder and Rosakis, 1988). Some results pertaining to the above issues and also to the variation of J and crack opening displacement will be given in Sec. 4.

The second issue that is addressed here (see Sec. 5), is the extent of regions over which plane strain and plane stress analyses provide a good approximation to the actual three dimensional fields. To this end, detailed three-dimensional and two-dimensional numerical calculations have been performed (see Sec. 2). These calculations model the monotonic loading of a ductile three point bend specimen from contained yielding to fully plastic conditions. The radial and angular variation of the stresses from these analyses will be compared with the HRR solution in the spirit of Shih and German, (1981), McMeeking and Parks (1979) and Narasimhan and Rosakis (1988), with the view of assessing J-dominance. Some preliminary results pertaining to the above issues have been discussed by Narasimhan, Rosakis and Zehnder, (1988).

2. NUMERICAL ANALYSIS

The three-point bend specimen shown in Fig. 1a, was modelled using three dimensional finite elements. The geometry of the mesh is shown in Fig. 1b. Due to symmetry, only one quarter of the specimen was simulated, with appropriate boundary conditions imposed on the

planes of symmetry. The mesh consists of 5 layers of elements (through *half the thickness* of the plate). Each layer is composed of 420 eight-noded brick elements. The layer interfaces are located at $x_3/h = 0, 0.15, 0.275, 0.375, 0.45$ and 0.5. It should be noted that the layers become thinner as the free surface is approached in order to model the corner singularity. The layer of elements adjoining the mid-surface of the plate is three times as thick as the one near the free surface.

The crack tip elements are formed by collapsing the eight noded brick elements to triangular prisms. The details of the *in-plane mesh* near the crack tip is shown in Fig. 1c. This fine mesh is composed of a circular region whose radius is equal to the thickness of the plate. There are ten circular rings in this region, which are divided by 19 rays at equal angular intervals of 10°. The radius of the innermost ring of elements (nearest to the tip) is 1/100 of the plate thickness. This detailed mesh is expected to provide sufficient resolution near the crack tip, so that a careful study of the asymptotic stress and strain variations may be performed.

Two dimensional plane strain and plane stress calculations were also performed with the same in-plane mesh (Fig. 1b) to obtain upper and lower bounds for the 3 dimensional calculations.

A small strain, J_2 incremental plasticity theory was used. The material was assumed to be homogeneous, isotropic and to obey the Huber-Von Mises yield criterion. The response of the material in uniaxial tension was characterized by a piecewise power hardening law of the form:

$$\frac{\varepsilon}{\varepsilon_o} = \begin{cases} \sigma / \sigma_o & \sigma \le \sigma_o \\ (\sigma / \sigma_o)^n & \sigma > \sigma_o \end{cases} \tag{2.1}$$

with a hardening exponent n = 22 and yield stress σ_0 = 1030 Mpa. These values were chosen to match the constitutive properties of the particular heat treatment of 4340 carbon steel used in the experiments. These experiments are described in detail in part II of this investigation.

The B-bar method proposed by Hughes (1980) and later modified by Nakamura, Shih and Freund (1986) was used to relieve artificial mesh locking effects that occur under nearly incompressible conditions (in the fully plastic range) under plane strain and in three dimensions. Nakamura, Shih and Freund (1986a) and (1986b) suggested that the B-bar method should be used with a stabilization procedure akin to Belytschko and Tsay (1983) to safeguard against a

spurious pressure mode. As recommended in Nakamura, Shih and Freund (1986), a stabilization parameter of 0.05 was used in the present calculations.

The stress computations were performed using the tangential predictor-radial return method with subincrementation (see appendix of Narasimhan and Rosakis 1988). The nonlinear finite element equilibrium equations were solved incrementally using a quasi-Newton method (BFGS) (Matthies and Strang, 1979). For the three-dimensional case, this method provided substantial savings as compared with the full Newton method. The convergence to an equilibrium solution was quite rapid in the early part of the load history, requiring typically 3 or 4 iterations in each load step. But it was quite slow as fully plastic conditions (given by the rigid plastic limit load) were approached. As suggested in Matthies and Strang (1979), a BFGS update was not performed whenever the condition number of the updating matrix became very large (greater than 10^5). This happened quite frequently when the limit load was approached. Also, smaller load increments were used near the limit load.

3. DESCRIPTION OF EXPERIMENTS

As described in detail in part II, the experiments were performed on three point bend specimens of a ductile 4340 steel with dimensions given in Figure 1a. Two specimens were tested. In both cases, the applied load and the load point displacement were measured and recorded during the experiments. In order to provide additional comparison between the numerical calculation and the experiments, a measurement of the out of plane displacement fields of the specimen surface was performed using Twyman-Green interferometry.

4. RESULTS

4.1 Load-Displacement Curves

The variation of load versus load point displacement is shown in Fig. 2 from the three dimensional and two dimensional numerical calculations. For comparison, the experimental load-displacement records for two specimens are shown in the figure up to the point of fracture initiation. The plane stress and plane strain limit loads (for a rigid-perfectly plastic material)

are also indicated in the figure. The curve obtained from the 3-D analysis lies in-between the curves from plane stress and plane strain calculations, and is much closer to plane stress. Also, very good agreement can be seen between the experiments and the 3-D computation.

4.2 The J Integral

The J integral defined by Rice (1968) for a two dimensional cracked body is path independent for a material obeying the small strain deformation theory of plasticity. Under the above conditions, this integral may be interpreted as the energy release rate and is also a characterizing parameter of the asymptotic crack tip fields (Hutchinson, 1968 and Rice and Rosengren, 1968).

For a three-dimensional crack, the J integral is defined over a cylindrical surface (Budiansky and Rice 1973, and Broberg 1987) surrounding the *entire* crack front. The numerical computation of the above surface integral in a 3-D finite element analysis is very difficult. However, the surface integral may also be interpreted as the energy released due to a unit (normal) virtual crack extension along the *entire* crack front. An *average* value, denoted here by J, can then be obtained by dividing the above quantity by the length of the crack front. (Nakamura, Shih and Freund, 1986 and Delorenzi and Shih, 1983).

If $\delta l(s)$ denotes the crack advance at a point s along a three dimensional crack front (in a direction normal to it) and ds the elemental arc length along the crack front, a local quantity $\hat{J}$ (x_3 / h) has been defined by Li, Shih and Needleman (1985) and Shih, Moran and Nakamura, (1986):

$$\frac{1}{h} \int_{-1/2}^{1/2} \hat{J}\,(x_3/h)\, \delta l(x_3 / h)\, dx_3 = -\delta\Pi$$

Here $\delta\Pi$ is the change in potential energy of the body. It has been (heuristically) argued, see for example Li, Shih and Needleman (1985) and Shih, Moran and Nakamura (1986) that $\hat{J}(s)$ plays a role of characterizing parameter (or amplitude factor) of the crack tip fields provided plane strain conditions prevail through the thickness as the crack front is approached and assuming that proportional loading is pointwise enforced. As noted earlier, this argument can be accepted only after a complete investigation of the three-dimensional near-tip fields validates

the above assumptions.

A domain integral representation of J and $\hat{J}(s)$ has been discussed by Li, Shih and Needleman (1985), Shih, Moran and Nakamura, (1986), Nakamura, Shih and Freund (1986a), and Nakamura, Shih and Freund (1986b). This method can be easily implemented in a finite element program and has also been found to give very accurate results. In particular, it is very effective in computing the near-tip value of J. This method was employed in the present analysis to calculate J from the numerical solution.

The variation of J versus the applied load is shown in Fig. 3a. Also shown in the figure is the J versus applied load record calculated from the experimental result on the basis of measured load-displacement curves (see Part II). In Fig. 3b, J is plotted against the load point displacement. It should be observed that the curve corresponding to the 3-D solution is again bounded by the plane strain and plane stress curves. For small load levels, the three analyses show results which are not very different from each other. These values also agree very well with J calculated on the basis of small scale yielding. Also, J from the 3-D analysis is close to the plane stress solution for the entire load range, except very near the plane stress limit load.

It is worth emphasizing here that the global 3-D specimen behavior such as the load displacement and the average J integral records (see Fig. 2, 3) are closer to the plane stress rather than plane strain approximations. This is not surprising given that the ratio of thickness to the in-plane dimensions of the specimen were relatively small.

Nevertheless as will be shown in the following section, at the vicinity of the crack tip, there is a strong variation of fields through the thickness which indicates the need for a 3-D analysis for the study of crack initiation. In Fig. 4, $\hat{J}$ normalized by J is plotted against normalized distance, x_3 / h, along the crack front for different ratios of the applied load P to the *plane stress limit load* P_o. The variation for the elastic case is also shown in the figure. It is seen that with increasing plastic deformation, there is a considerable variation of $\hat{J}$ through the thickness with the value at the center being much higher than that at the free surface. Similar trends have been reported in Nakamura, Shih and Freund (1986a) and Delorenzi and Shih (1983).

4.3 Crack Tip Opening Displacement

The crack tip opening displacement was calculated from the numerical solution using the 45° intercept procedure introduced by Shih (1981). The crack tip opening displacement at the centerline of the 3-D specimen is plotted against the load in Fig. 5. The plane stress and plane strain results are also shown in the figure for comparison. As before, the 3-D curve is bounded by the 2-D analyses.

The variation of the crack tip opening displacement along the crack front is shown in Fig. 6 for three different load ratios P/P_o. The crack tip opening displacement, δ_t has been made dimensionless by the value δ_{CL}, at the centerline of the specimen. As in the case of $\hat{J}$ in Fig. 4, There is a strong variation of the crack tip opening with increasing plastic deformation, with the value at the centerline being very much in excess of that at the free surface. Such strong variation of crack tip opening through the thickness was also observed in Delorenzi and Shih (1983) and Wellman, Rolfe and Dodds (1987). This result along with Fig. 4 suggests the possibility of a tunneling mode of fracture with the crack beginning to propagate first at the center. Indeed, some evidence of this could be seen by a post mortem examination of the fracture surface of the experimental specimen. In Fig. 7, the crack opening displacement at the center of the specimen, which is normalized by (J/σ_o) is plotted against the quantity $J/(\sigma_o C)$. Here C is the uncracked ligament length. The 2-D results are also shown in the figure. The dimensionless quantity $J/(\sigma_o C)$ is an indication of the extend of plastic yielding (Shih, 1981 and Shih and German, 1981). Small values of $J/(\sigma_o C)$ (less than about 0.001) indicate well-contained yielding, while large values (greater than 0.01) correspond to large scale plasticity.

The values of $\delta_t/(J/\sigma_o)$ based on the 2-D solutions are fairly constant over the entire range of plastic deformation. For plane stress, $\delta_t/(J/\sigma_o)$ varies from 0.82 for well contained yielding to about 0.80 for large scale plasticity, while for plane strain it varies from 0.62 to about 0.60. These values are somewhat smaller than the HRR solution which gives 0.95 and 0.68 for plane stress and plane strain respectively corresponding to n = 22 (Shih, 1981 and Shih, 1983).

However, Narasimhan and Rosakis (1988), reported a value of $\delta_t/(J/\sigma_o)$ of 0.85 for the non-hardening case based on a finite element solution which modelled plane stress, small scale yielding conditions. Shih (1981) has also computed the crack opening displacement for different hardening exponents and specimen geometries based on plane strain finite element

solutions. For the Cracked Bend Bar (of perfectly plastic material), he reports a value of $\delta_t/(J/\sigma_o)$ which varies from 0.65 to 0.58 from contained yielding to fully plastic conditions. As noted in Narasimhan and Rosakis (1988), the discrepancy with the HRR solution *in the non-hardening limit* is due to the fact that the HRR strain solution may not dominate over any finite distance near the tip.

It can be seen from Fig. 7 that the normalized crack opening displacement, $\delta_t/(J/\sigma_o)$ at the centerline of the 3-D specimen varies from about 0.68 for contained yielding to about 0.75 for large scale yielding. For contained yielding, this value is closer to plane strain whereas for large scale yielding is closer to the plane stress limit. A qualitatively similar trend may be noticed in the results obtained in Delorenzi and Shih (1983) for a compact tension specimen.

4.4 Stress Variation Through the Thickness

The variation of the plane strain constraint (as given by the ratio $\sigma_{33}/(\sigma_{11} + \sigma_{22})$ through the thickness of the specimen is shown in Fig. 8 for different load ratios P / P_o. The distribution for the elastic case is also plotted in the figure. The stresses in this plot were evaluated at the centroid of the elements *nearest* to the tip, located at r/h = 0.005 and $\theta = 0°$.

The first observation that can be made is that the ratio $\sigma_{33}/(\sigma_{11} + \sigma_{22})$ is uniform over most of the specimen thickness (along the crack front) and drops to zero very near the free surface. Its value in the interior of the specimen is about 0.28 for the elastic case and approaches 0.47 with increasing plastic deformation. It should be noted here that under plane strain conditions $\sigma_{33}/(\sigma_{11} + \sigma_{22})$ is equal to the Poissons ratio (which is 0.3 in the present analysis) for the elastic case. Also this ratio is equal to 0.5 in the fully plastic limit.

Secondly, the numerical results indicate that even for an applied load of only 0.45 P_o the ratio $\sigma_{33}/(\sigma_{11} + \sigma_{22})$ near the crack front is 0.46 in the interior of the specimen. The ratio shows very little variation with increase in load level. This is due to the low hardening of the material which allows very large in-plane plastic strains to accumulate near the tip even for moderate extents of yielding. This leads to a stress distribution near the crack front in the interior of the specimen which is similar to the plane strain Prandtl field, (see Rice and Rosengren, 1968, and Rice, 1968), also see Sec. 4 and Fig 22. The observation that $\sigma_{33} / (\sigma_{11} + \sigma_{22})$ approaches the value 0.5 near the crack front, is consistent with the expectation of a plane strain

like constraint in the center plane of the specimen.

The variation through the thickness of the cartesian stress components σ_{11}, σ_{22} and σ_{33}, normalized by the yield stress σ_o, is shown in Figs. 9, 10, and 11 for three different load levels ranging from contained yielding to large scale plasticity. The stresses displayed in these figures are computed at $\theta = 0°$ and r/h = 0.005, 0.025, 0.065, 0.125, 0.205, 0.305, 0.425 and 0.565. The arrow direction in the figures indicates increasing r/h values. The distribution through the thickness of the normalized triaxial stress $(\sigma_{11} + \sigma_{22} + \sigma_{33}) / 3\sigma_o$ is also shown in these figures.

It can be observed that very near the crack front (in the interior of the specimen) the stresses are highly elevated above the yield stress leading to a strongly triaxial stress field. This is characteristic of the plane strain crack tip fields (Rice and Rosengren, 1968, and Rice, 1968). For low load levels (Fig. 9), the stress variation along the crack front is uniform over most of the specimen thickness and drops near the free surface. But in the fully plastic limit (Fig. 11) a strong variation of stresses along the crack front is noticed. This leads to a *considerable loss of triaxiality* as the free surface is approached along the crack front. This observation is important since a strongly triaxial field influences the growth and nucleation of voids.

These figures show that for r/h > 0.5, σ_{33} is close to zero uniformly over the specimen thickness irrespective of the load level. Also, the other stress components have very little variation through the thickness for r/h > 0.5. This suggests that plane stress conditions are approached for distances from the crack front in excess of half the specimen thickness (see Sec. 5 for further discussion).

4.5 Surface (out-of-plane) displacements

Two views of the surface displacement field u_3 of the deformed specimen at a load of 52300 N (obtained from the numerical calculation) are shown in Fig. 12. The out-of-plane surface displacements of Fig. 12 were used to generate numerical interferograms for comparison with the experimental results described in Part II. Figure 13 is a composite picture showing one-half of an experimental and one-half of a numerically generated interferogram. As is evident from this comparison, good qualitative agreement of experimental and synthetic interferograms is achieved. In Fig. 14, the numerical and experimental out-of-plane displacements along

the ray ahead of the cracktip, u_3 (r, $\theta = 0$), are plotted against normalized distance from the tip at a load of 52300 N. The displacements have been made dimensionless by the quantity (J/σ_o). The extent of the plastic zone ahead of the tip as well as the location along the x_1 axis corresponding to half the specimen thickness are indicated for reference. The out-of-displacement corresponding to the plane stress HRR field at the same average J value is also plotted for comparison.

It can be observed that there is excellent agreement between the 3-D numerical and experimental results, even very near the crack tip. The agreement was found to be very good over the entire range of loading (see part II). It was found that the plane stress HRR field did not adequately describe u_3 on the specimen surface. The above observation has also been made during previous experimental investigations using the optical method of caustics (Rosakis, Zehnder and Narasimhan, 1987 and Zehnder, 1987). In these studies, it was noticed that caustics based on plane stress HRR fields could not always be used to accurately measure J. This discrepancy is because of three dimensionality near the crack tip and due to finite specimen dimensions that cause higher order terms to become important away from the crack tip. Further comparisons between numerical and experimental results based on caustics and interferometry may be found in Part II.

5. THREE DIMENSIONAL EFFECTS AND HRR DOMINANCE

5.1 Radial Stress Variation

The radial variation of the normalized opening stress, σ_{22} / σ_o, along the uncracked ligament obtained from the *plane stress* and *plane strain* numerical solutions, are displayed in Figs. 15 and 16 respectively. Results are given for three load levels ranging from well contained yielding to large scale plasticity. The extent of plastic deformation is indicated by the parameter $C\sigma_o/J$ (see Sec. 4.3). The stress distribution based on the HRR field is also shown in these figures.

It can be seen from Fig. 15 that in the case of plane stress, the HRR stress field agrees very well with the numerical solution over a large distance (x_1 less than about 30 J/δ_o) for all levels of plastic deformation. A similar observation was made in Narasimhan and Rosakis (1988) for

plane stress, small scale yielding conditions. Hence it appears that under plane stress, HRR dominance is assured for distances along the ligament of the order of 30 to 40 times the crack tip opening displacement δ_t.

The radial stress distribution for plane strain (Fig. 16) suggests that the HRR field dominates only very near the tip (for x_1 less than about 3 J/σ_o). This is in good agreement with the results of Shih and German (1981) for the Cracked Bend Bar. Thus, as noted in Shih and German (1981), HRR dominance to about 6 to 10 δ_t for all levels of plastic yielding.

The radial variation of the three dimensional normalized out-of-plane stress component $\sigma_{33} / (\sigma_{11} + \sigma_{22})$ (which is an indication of the plane strain constraint) ahead of the crack front is shown in Fig. 17 along three different planes through the specimen thickness. These planes correspond to x_3 /h of 0.075 (which is near the mid plane of the specimen), 0.325 (near the quarter plane) and 0.475 (near the free surface). These results have been taken from the 3-D numerical solution at applied load levels of $0.45P_o$, $0.7P_o$ and P_o.

As noted earlier(in connection with Fig. 8), it can be seen from this figure that the ratio $\sigma_{33}/(\sigma_{11} + \sigma_{22})$ approaches a value close to 0.5 near the crack tip over most of the specimen thickness once moderate amounts of yielding take place. Also, irrespective of load level and for all planes through the thickness, the above ratio becomes quite small for radial distances from the crack tip exceeding approximately half the specimen thickness ($r > 0.5$ h). This observation along with Figs. 9, 10 and 11, which show that the other stress components have negligible variation through the thickness for $r/h > 0.5$, suggests that plane stress conditions are approached for distances from the crack tip exceeding half the specimen thickness. A similar conclusion was reached by Yang and Freund (1984) on the basis of an analytical investigation and by Parsons, Hall and Rosakis (1986), on the basis of a numerical study of 3-D, elastic cracked specimens. Experimental observations based on the optical method of caustics (Rosakis and Ravichandar, 1984, and Rosakis, Zehnder and Narasimhan, 1987), also indicate that three dimensional effects become important only for $r/h < 0.5$.

In order to examine the above issue further, the radial distribution of the normalized opening stress σ_{22} / σ_o ahead of the crack front is shown along three different planes through the specimen thickness $x_3 / h = 0.075$, 0.325 and 0.475) in Fig. 18. The bottom scale in the figure gives the radial distance from the tip normalized by the specimen thickness h, while in the top scale

the normalization is done with respect to the uncracked ligament length C. For comparison, the corresponding variation based on the full field plane stress and the full field plane strain numerical solutions (at the *same load level* P) are indicated in the figure. Results are once again provided for three values of applied load.

This figure shows that for r/h > 0.5, the plane stress radial stress distribution is approached over the entire specimen thickness irrespective of the load. On the other hand, the plane strain radial stress variation provides a good approximation near the mid-plane of the specimen for r/h < 0.2. It should be noted that the σ_{22} (opening stress) distribution is highly elevated above the yield stress as the crack tip is approached in the interior of the specimen. Also, it can be seen that there is substantial variation of stresses through the thickness as fully plastic conditions are approached (see Fig. 11 and distribution corresponding to $P = P_o$ in Fig. 18).

In Fig. 19, the radial variation of the opening stress ahead of the crack tip is again shown in the same non-dimensional scales but is now compared with the analytical asymptotic plane stress and plane strain HRR distributions. The asymptotic (HRR) distributions corresponding to the same average value of J have been plotted in this figure. This figure demonstrates that very near the crack tip (r < 0.02 h) the opening stress in the interior of the specimen tends towards the asymptotic plane strain HRR solution. On the other hand, the plane stress HRR solution is approached away from the crack tip within the plastic zone. This is more evident with increasing plastic yielding (see figures corresponding to $P = 0.7P_o$ and $P = P_o$).

5.2 Angular stress variation

The angular variation of stresses in the ring of elements closest to the crack tip ($r = 0.005\,h = 0.001C$) obtained from the plane stress and plane strain numerical solutions is displayed in Figs. 21 and 22 respectively. The stresses in these plots have been normalized by the maximum value of the equivalent stress $\bar{\sigma} = (\frac{3}{2} S_{ij} S_{ij})^{1/2}$. Th angular stress variation given by the HRR solution is also shown in these figures for comparison. The values of the load ratios P/P_o and the dimensionless quantity $r/(J/\sigma_o)$ are also indicated in the figures. It can be seen that the near-tip two-dimensional numerical results display very good agreement with the corresponding HRR distribution for the entire loading range.

In Fig. 22, the near-tip angular distribution of the normalized stresses obtained from the 3-D numerical solution at $x_3 = 0.075\,h$ (near the mid-plane of the specimen) and $r = 0.005\,h$ is shown. Results are given for three different load ratios P/P_o. Also plotted in the figure is the angular stress variation given by the plane strain HRR asymptotic solution. It is found that the 3-D crack tip stresses near the mid-plane of the specimen agree very closely with the plane strain HRR field.

It should be recalled that the material used in the experiments, and modeled by the numerical calculations, has a very low strain hardening ($n = 22$) and hance the angular stress variation in Fig. 22 displays all the essential features of the perfectly-plastic plane-strain Prandtl slip line field. For example, in the angular range $45° < \theta < 135°$, $\sigma_{rr} = \sigma_{\theta\theta}$ and $\sigma_{r\theta}$ is constant. These are characteristic of the "centered fan" region of the Prandtl field (Rice, 1968) where the plastic strains are singular as $1/r$. Also, note that the stresses are highly elevated (above $\bar{\sigma}_{max}$) ahead of the crack tip ($\theta = 0°$). This result clearly demonstrates the dominance of the plane strain HRR field along the crack front in the interior of the specimen.

5.3 Plastic zones

The plastic zones corresponding to the two different load levels and three different planes through the specimen thickness ($x_3/h = 0.075, 0.325$ and 0.475) are shown in Figures 23 and 24.

Both figures display contours of equal equivalent stress $\bar{\sigma}$. The contour further away from the crack tip (boundary of the zones) corresponds to $\bar{\sigma} = 0.99\,\sigma_o$. The remaining contours correspond to $\bar{\sigma} = 1.02\,\sigma_o$, $1.05\,\sigma_o$, $1.08\,\sigma_o$, $1.11\,\sigma_o$, respectively. Figure 23 corresponds to $P = 0.7\,P_o$. For this load level, the plastic zone has not yet interracted with the applied loads at the boundary. For all cross sections, the maximum plastic zone site is less than half the specimen thickness and thus it lies well within the region of high near tip three dimensionality as discussed in section 5.1. It is somewhat surprising to note here that the plastic zone shape obtained at the specimen *surface* looks closer to the *plane strain* plastic zone shape than its counterpart in the middle. This contradicts the popular concept of plastic zone shapes as reported in a number of books on fracture mechanics, (Hellan, 1985, Kanninen and Popelar, 1985).

Figure 24 shows contours of $\bar{\sigma}$ for $P = P_o$. The figure clearly indicates the interractions of the crack tip plastic zone with the plastic deformation at the specimen boundary due to the applied loads. In this case and for all cross sections, the outer contour of equal $\bar{\sigma}$ reveals almost circular plastic zone shapes reminiscent of the shapes predicted by Narasimhan and Rosakis (1988), on the basis of a plane stress analysis. This is not surprising since the elastic plastic boundary now lies well outside a circle of radius $h/2$ (dotted line) which signifies the region outside which plane stress conditions dominate. Indeed, as shown in figure 17, the stress field for all load levels, approaches the plane stress constraint for $r/h > 0.5$.

6. CONCLUSIONS

A simultaneous experimental and numerical (both 3-D and 2-D) investigation has been performed to simulate the monotonic loading of a ductile 3-point bend specimen from contained to fully plastic conditions. The average J and the crack tip opening displacement from the 3-D analysis are bounded by the 2-D (plane stress and plane strain) analyses. The cracktip opening displacement and stresses exhibit a strong variation along the crack front with increasing plastic deformation. The 3-D numerical results clearly indicate that the plane strain HRR field dominates very near the crack front ($r < 0.02\,h$) in the *interior* of the specimen. On the other hand, the plane stress HRR field agrees well with the 3-D numerical results obtained on the surface layer of elements. The near-tip angular stress variation close to the mid-surface of the specimen displays all the essential features of the asymptotic plane strain Prandtl field, once moderate amount of yielding has occurred.

On the other hand, there is a considerable loss in triaxiality of the stress field as the free surface is apporached along the crack front. This is particulary evident for the larger applied loads and suggests a tendancy towards loss of local J dominance along the crack front as large scale yielding conditions are approached. The radial and thickness variations of the stresses from the 3-D analysis suggests that for $r > 0.5\,h$, plane stress conditions are approached. Comparison of the results to 2-D analyses, whenever appropriate, and the excellent agreement between the numerical and experimental, $P - \delta$, $J - P$ and $u_3(r,\theta)$ results leave no question that the 3-D calculations are accurate. These comparisons also show that the calculation is sufficiently refined to model this specimen well, both in the overall behavior and in the details of the near-tip fields.

7. ACKNOWLEDGEMENTS

Support of the ONR contract N00014-85-K-0596 is gratefully acknowledged. The second author (A.J.Rosakis) also aknowledges the support of the NSF-PYI Grant MSM-8451204. The computations were performed using the Supercomputer facilities at the University of California at San Diego.

REFERENCES

Belytschko, T. and Tsay, C. S. 1983 "A Stabilization Procedure for the Quadrilateral Plate Element with One-point Quadrature," *International Journal for Numerical Methods in Engineering*, Vol. 19, pp. 405-419.

Broberg, K. B. 1987 "A Path Independent Integral for Plates," *Journal of Applied Mechanics* (Brief Notes), Vol. 54, pp. 458-459.

Budiansky, B. and Rice, J. R. 1973 "Conservation Laws and Energy-release rates" *Journal of Applied Mechanics*, Vol. 40, pp. 201-203.

Delorenzi, H. G. and Shih, C. F. 1983 "3-D Elastic Plastic Investigation of Fracture Parameters in Side-grooved Compact Specimen," *International Journal of Fracture*, Vol. 21, pp. 195-220.

Dodds, R. H., Carpenter, W. C. and Sorem, W. A. 1987 in *Proceedings of the Fourth International Conference on Numerical Methods in Fracture Mechanics*, edited by A. R. Luxmoore et al., pp. 283-297.

Hellan, K., 1985 "Introduction to Fracture Mechanics," McGraw-Hill.

Hughes, T.J.R., 1980 "Generalization of Selective Integration Procedures to Anisotropic and Nonlinear Media," *International Journal for Numerical Methods in Engineering*, Vol. 15, pp. 1413-1418.

Hutchinson, J. W. 1968 "Plastic Stress and Strain Fields at a Crack Tip," *Journal of Mechanics and Physics of Solids*, Vol. 16, pp. 337-347.

Hutchinson, J. W. 1983 "Fundamentals of the Phenomenological Theory of Non-linear Fracture Mechanics," *Journal of Applied Mechanics*, Vol. 50, pp. 1042-1051.

Kanninen, M.F. and Popelar, C., 1985, "Advanced Fracture Mechanics," Oxford University Press.

Li, F. Z., Shih, C. F. and Needleman, A. 1985 "A Comparison of Methods for Calculating Energy Release Rates," *Engineering Fracture Mechanics*, Vol. 21, pp. 405-421.

Matthies, H., and Strang, G., 1979, "The Solution of Non-linear Finite Element Equations," *International Journal for Numerical Methods in Engineering* Vol. 14, pp. 1613-1626.

McMeeking, R. M. and Parks, D. M. 1979 "On Criteria for J-dominance of Crack-tip Fields in Large-scale Yielding," in *Elastic-Plastic Fracture*, ASTM STP 668, pp. 175-194.

Nakamura, T., Shih, C. F. and Freund, L. B. 1986a "Analysis of a Dynamically Loaded Three-point-bend Ductile Fracture Specimen," *Engineering Fracture Mechanics*, Vol. 25, pp. 323-339.

Nakamura, T., Shih, C. F. and Freund, L. B. 1986b "Three-dimensional Transient Analysis of a Dynamically Loaded Three-point Bend Ductile Fracture Specimen," Brown University Report ONR 0365/3, to appear in ASTM STP #995.

Narasimhan, R. and Rosakis, A. J. 1988 "A Finite Element Analysis of small-scale Yielding Near a Stationary Crack Under Plane Stress," *Journal of Mechanics and Physics of Solids*, Vol. 36, no. 1, pp. 77-117.

Narasimhan, R., Rosakis, A.J. and Zehnder, A.T., "Three-dimensional Fields for a Through Crack in an Elastic-plastic Solid: Numerical Analysis and Comparison With Interferometric Measurements, 1988. ASME, AMD-Vol. 91 on "Analytical, Numerical and Experimental Aspects of Three-Dimensional Fracture Processes." A.J. Rosakis, K. Ravi-Chandar and Y. Rajapakse (Eds.).

Nicholas, P. J. and Luxmoore, A. R. 1987 in *Proceedings of the Fourth International Conference on Numerical Methods in Fracture Mechanics*, edited by A. R. Luxmoore et al., pp. 243-258.

Parsons, I.D., Hall, J.F. and Rosakis, A.J., 1986, "A Finite Element Investigation of the Elastostatic State Near a Three- Dimensional Edge Crack," Caltech Report SM 86.29.

Rice, J. R. 1968 "A Path Independent Integral and the Approximate Analysis of Strain Concentration by Notches and Cracks," *Journal of Applied Mechanics*, Vol. 35, pp. 379-386.

Rice, J. R. and Rosengren, G. F. 1968 "Plane Strain Deformation Near a crack Tip in a Power-law Hardening Material," *Journal of Mechanics and Physics of Solids*, Vol. 16, pp. 1-12.

Rosakis, A.J. and Ravichandar, K. 1986, "On Crack Tip Stress State: An Experimental Evaluation of Three- dimensional Effects." *International Journal of Solids and Structures*, Vol. 22, pp. 121-138.

Rosakis, A.J., Zehnder, A.T., and Narasimhan, R., 1987, "Caustics by Reflection and their Application to Elastic-plastic and Dynamic Fracture Mechanics," prepared for the SPIE Conference on Photomechanics and Speckle Metrology, San Diego, California, to appear in *Optical Engineering* (1988).

Shih, C. F. 1981 "Relationships Between the J-integral and the Crack Opening Displacement for Stationary and Extending Cracks," *Journal of Mechanics and Physics of Solids*, Vol. 29, pp. 305-326.

Shih, C. F. 1983 "Tables of HRR Singular Field Quantities," Brown University Report.

Shih, C. F. and German, M. D. 1981 "Requirements for One Parameter Characterization of Crack Tip Fields by the H.R.R. Singularity," *International Journal of Fracture*, Vol. 17, pp. 27-43.

Shih, C. F., Moran, B. and Nakamura, T. 1986 "Energy Release Rate Along a Three-dimensional Crack Front in a Thermally Stressed Body," *International Journal of Fracture*, Vol. 30, pp. 79-102.

Wellman, G. W. Rolfe, S. T. and Dodds, R. H. 1987 *Welding Research Council Bulletin*, Vol. 299, pp. 15-25.

Yang, W. and Freund, L. B. 1985 "Transverse Shear Effects for Through-Cracks in an Elastic Plate," *International Journal of Solids and Structures*, Vol. 21, pp. 977-994.

Zehnder, A.T. 1987 "Dynamic Fracture Initiation and Propagation in Metals: Experimental Results and Techniques," Ph.D. thesis, California Institute of Technology.

Zehnder, A.T. and Rosakis, A.J., 1988 "Three Dimensional Effects Near a Crack Tip in a Ductile Three Point Bend Specimen Part II: An Experimental Investigation Using Interferometry and Caustics", Caltech Report SM88-7, Submitted to the *Journal of Applied Mechanics*.

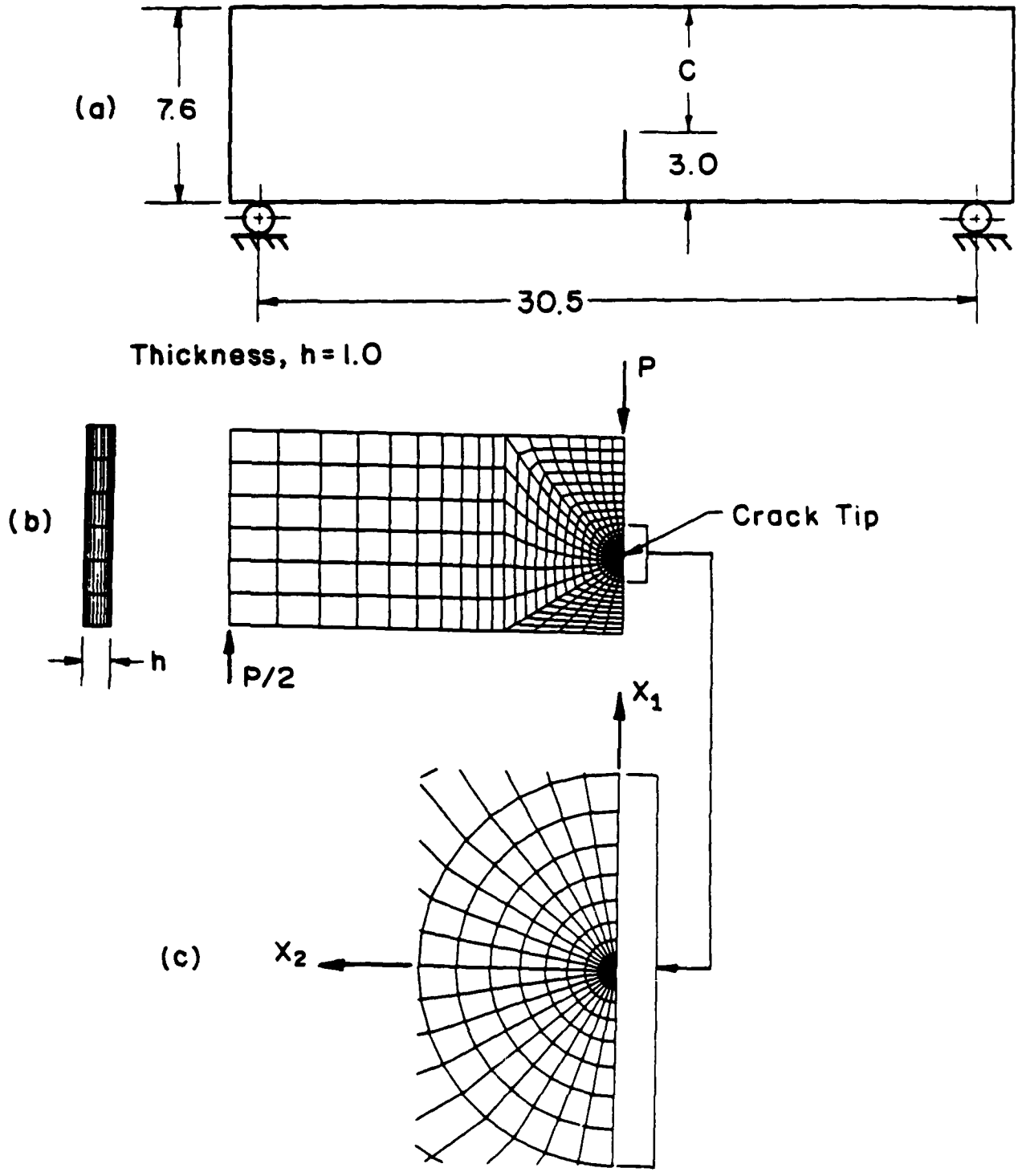

Figure 1.: (a) Test specimen geometry. All dimensions are in cm. (b) Mesh used in finite element analysis. (c) Details of in-plane mesh near the crack tip.

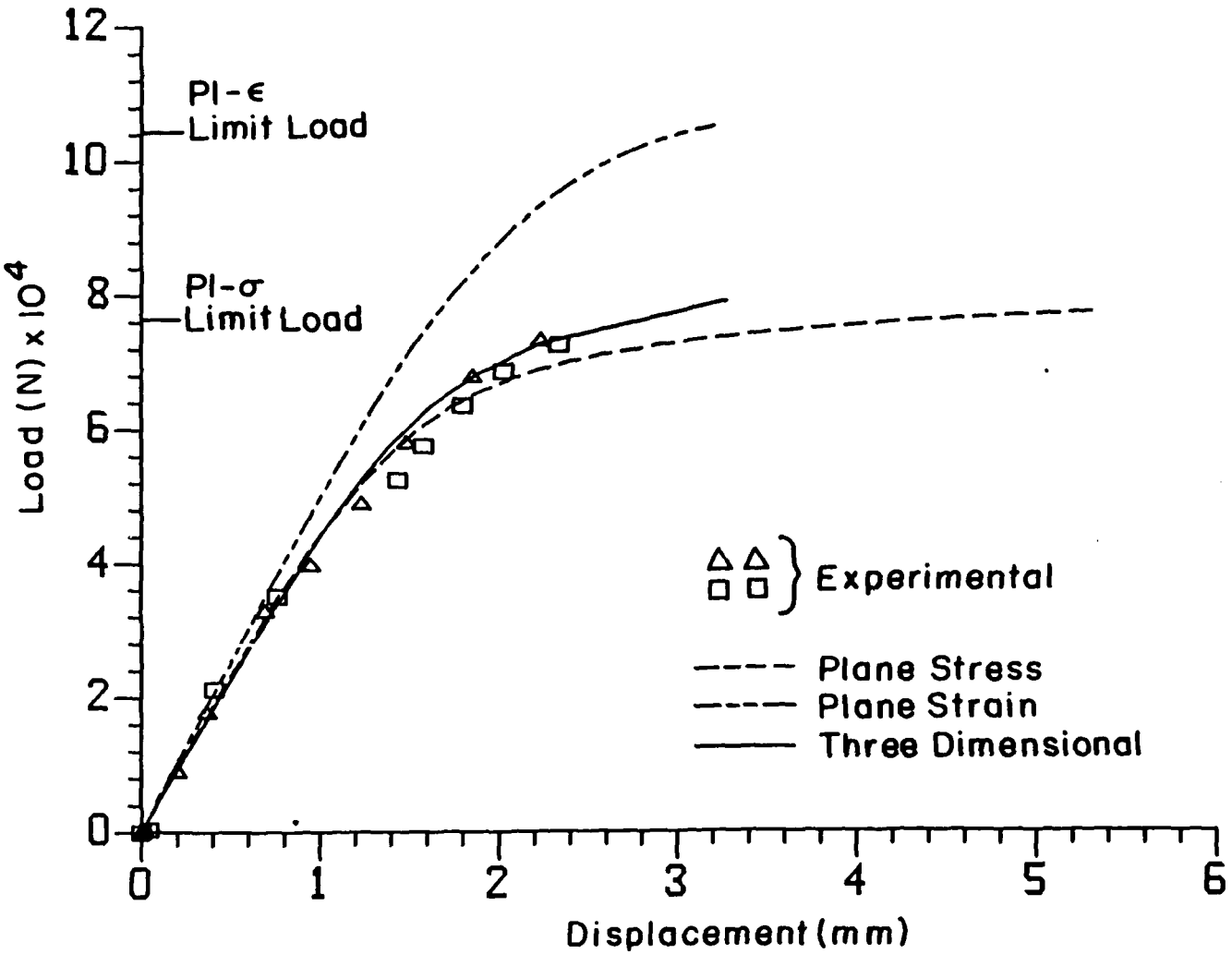

Figure 2.: Load - Load displacement curve.

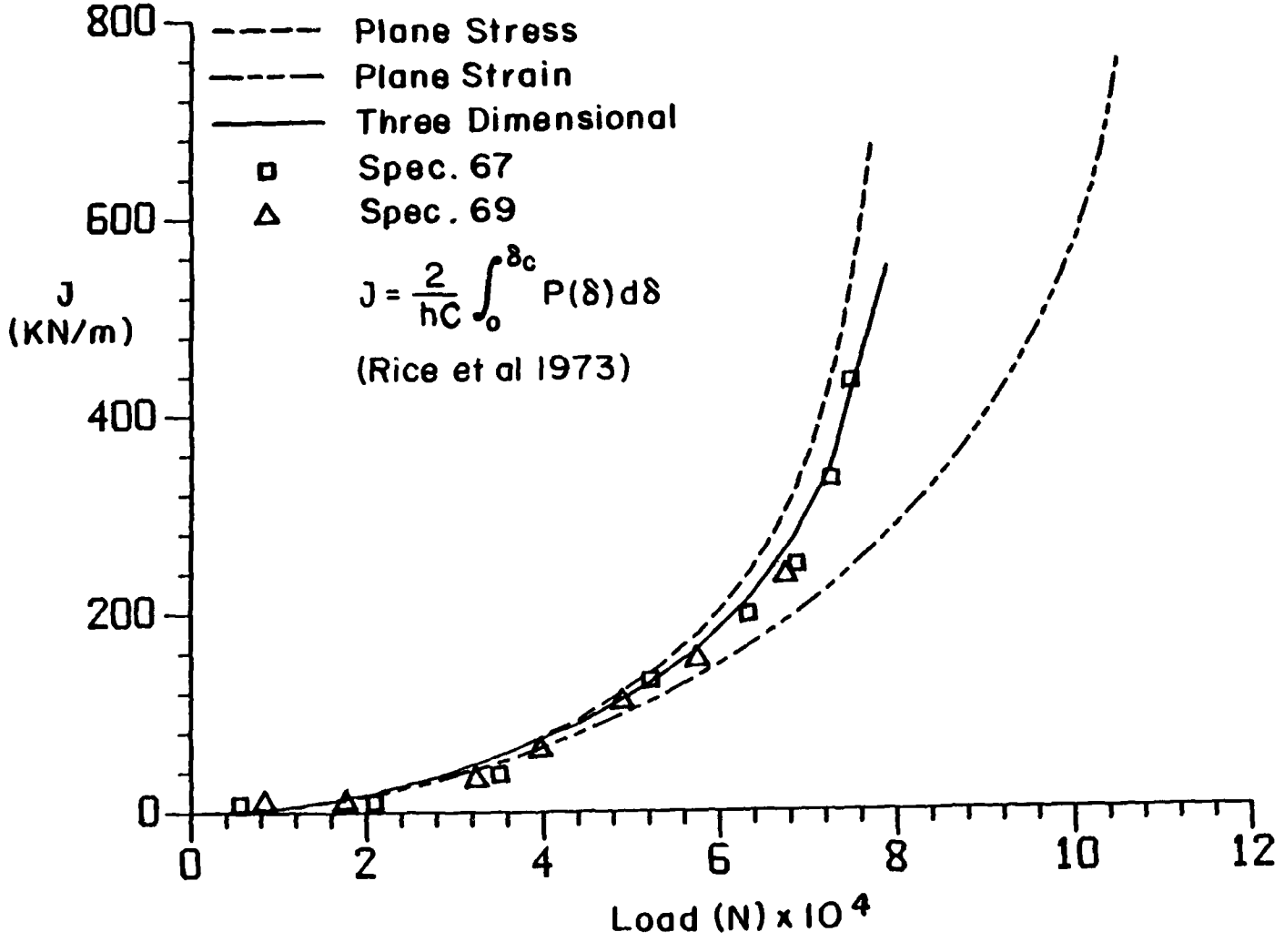

Figure 3a.: *J* versus applied load

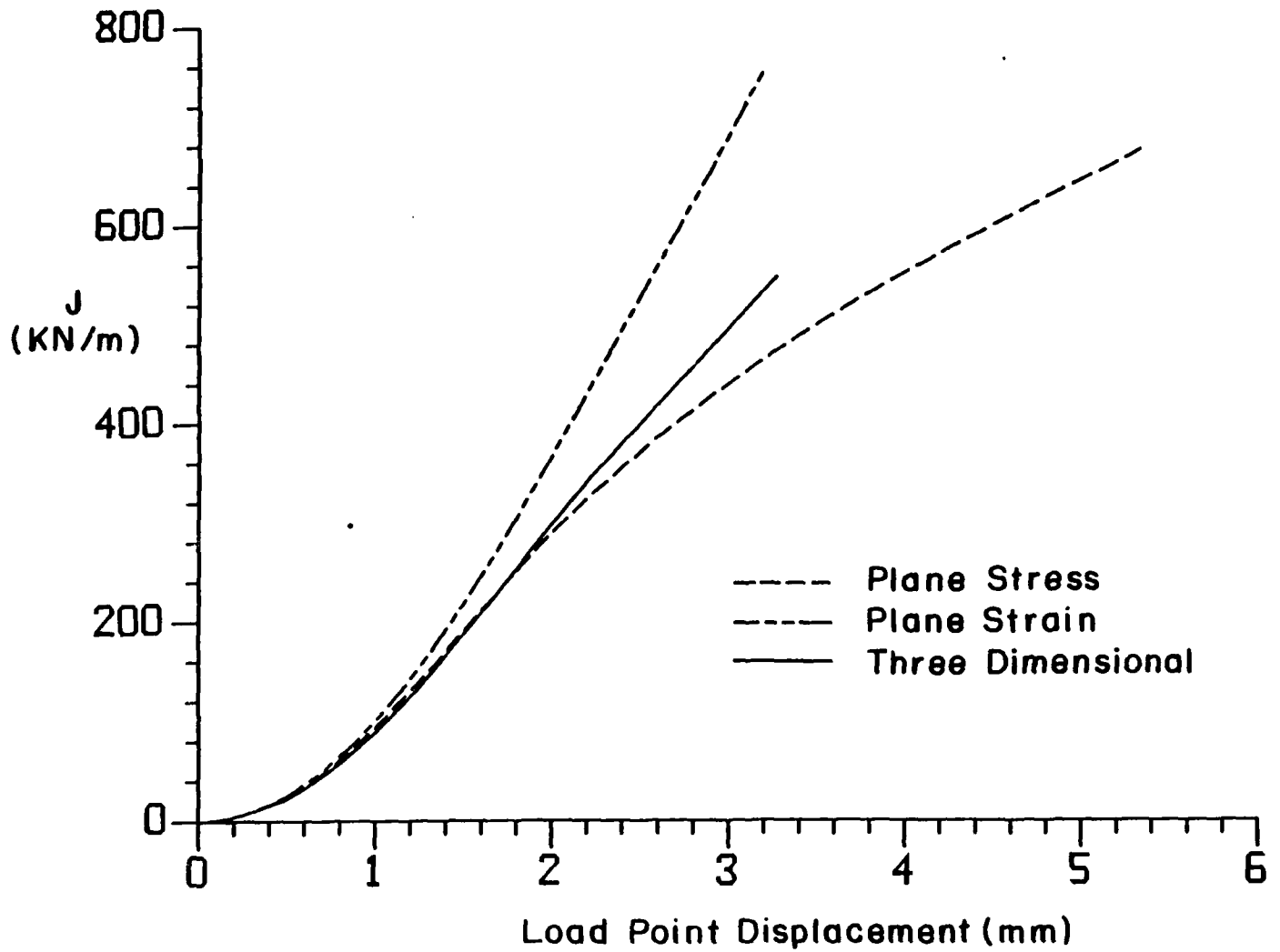

Figure 3b.: J versus load point displacement.

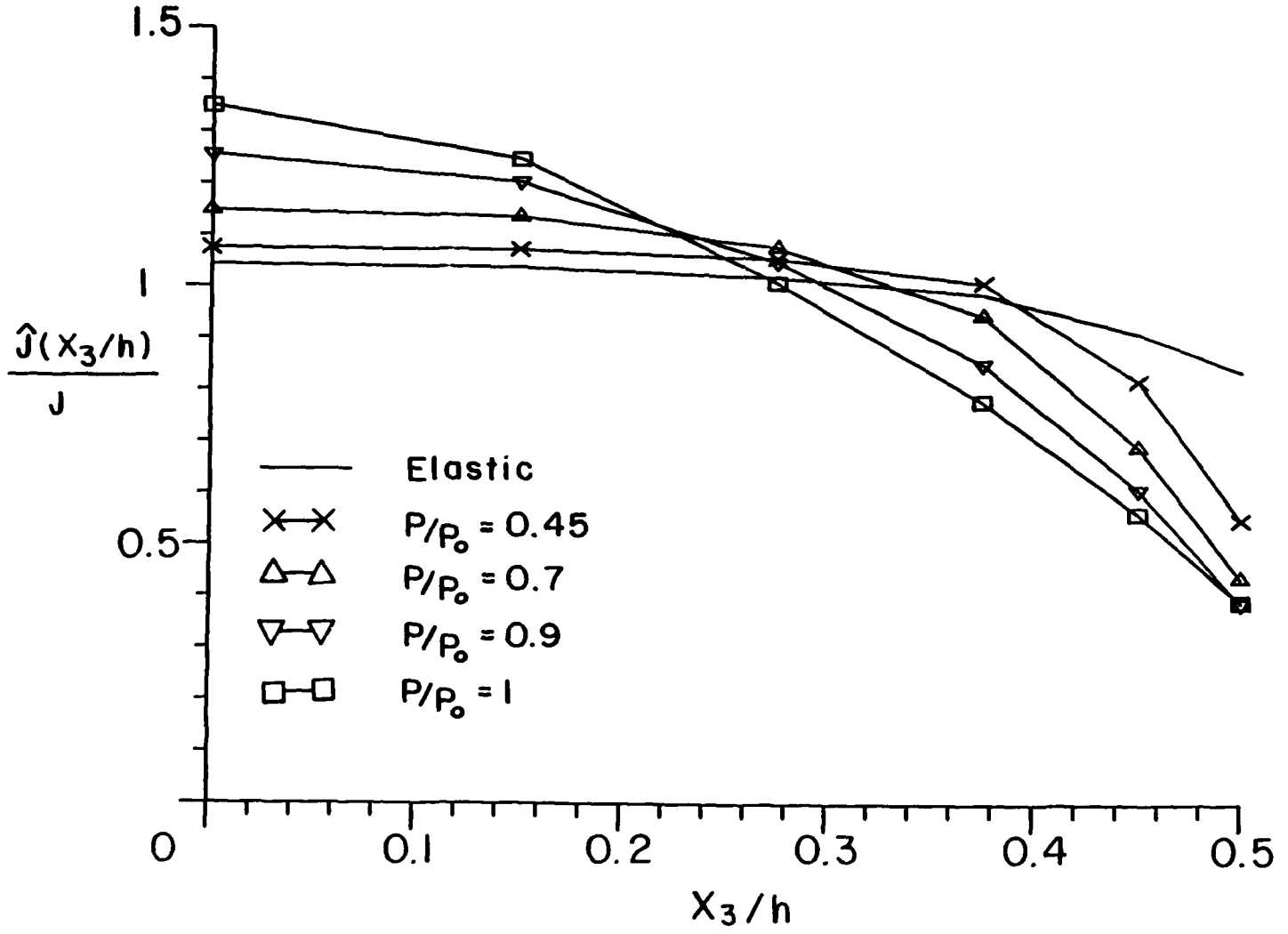

Figure 4.: Variation of $\hat{J}$ through the thickness for different load ratios. P_o is the plane stress limit load for a rigid-perfectly plastic material.

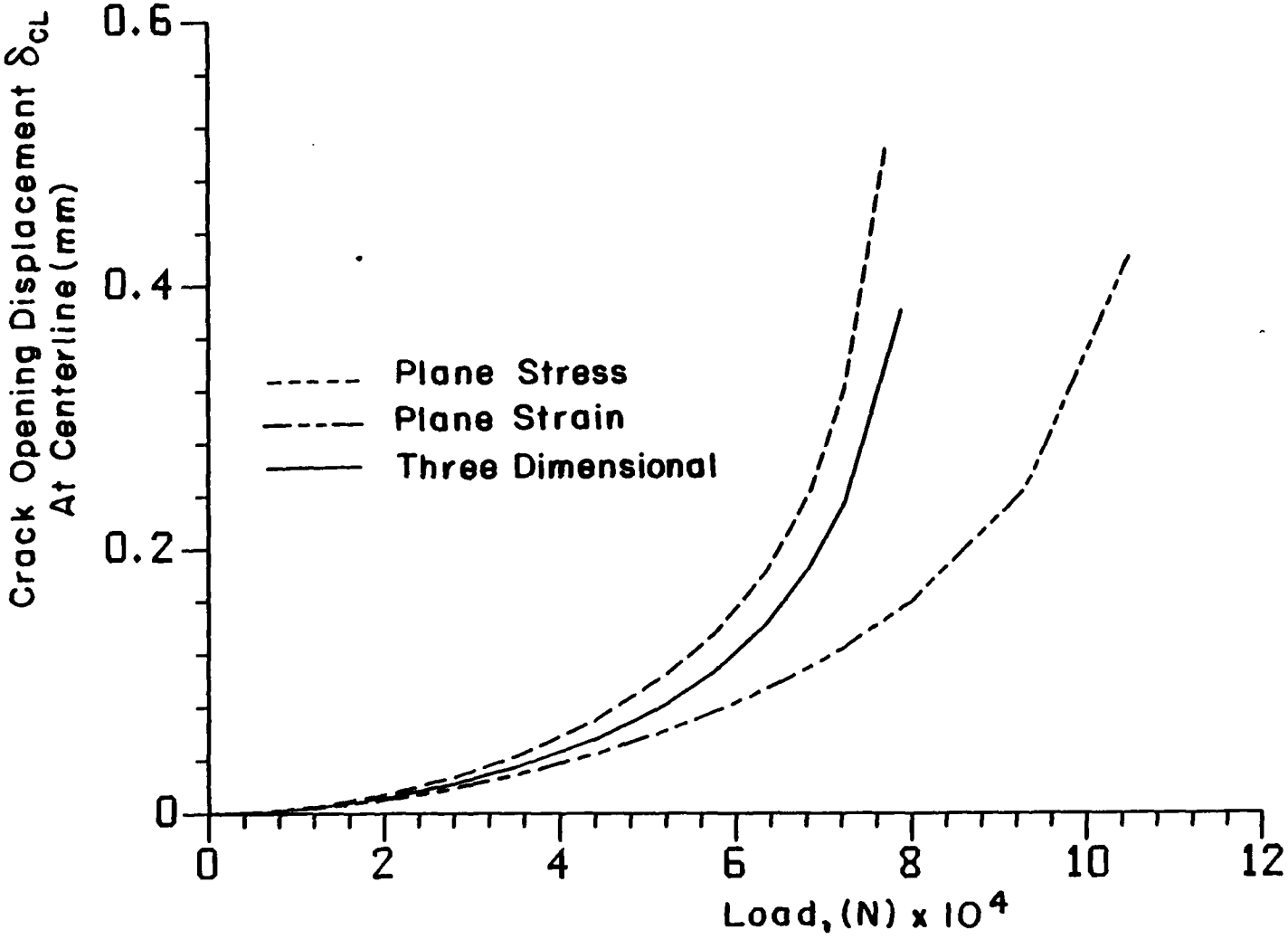

Figure 5.: Crack tip opening displacement at centerline versus load.

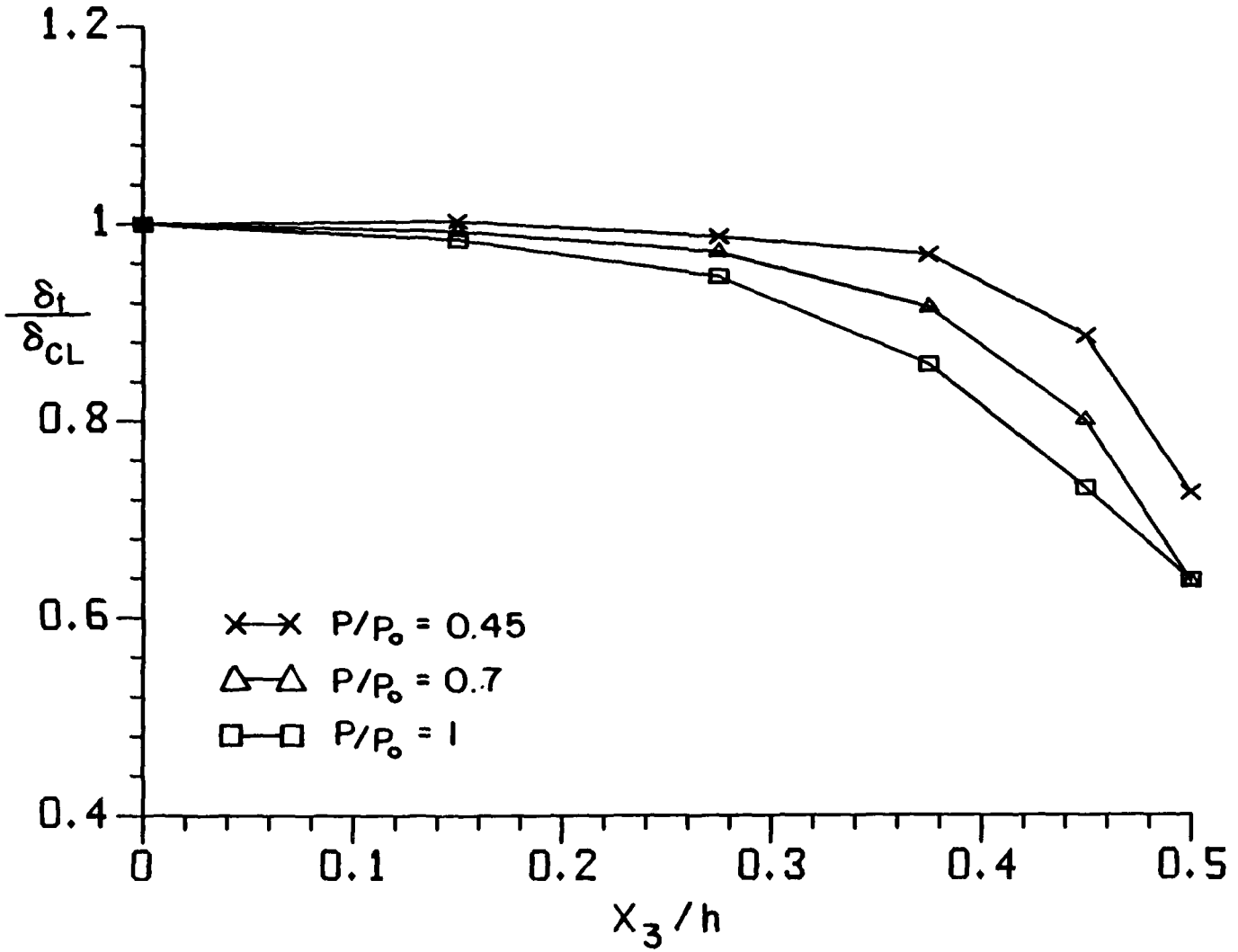

Figure 6.: Variation of the crack opening displacement along the crack front.

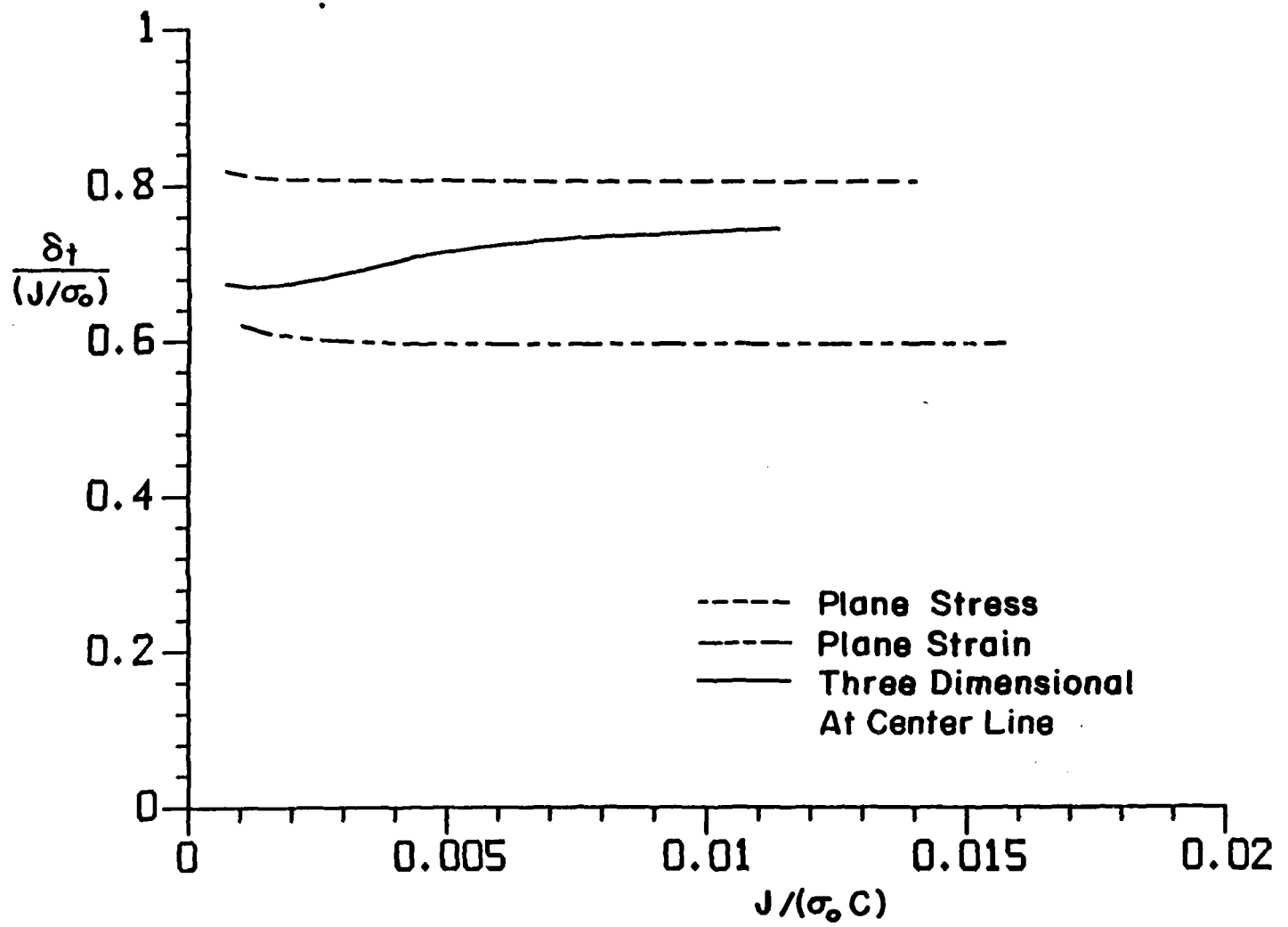

Figure 7.: Variation of the normalized centerline crack tip opening displacement $\delta_t/(J/\sigma_o)$ from contained yielding to fully plastic conditions.

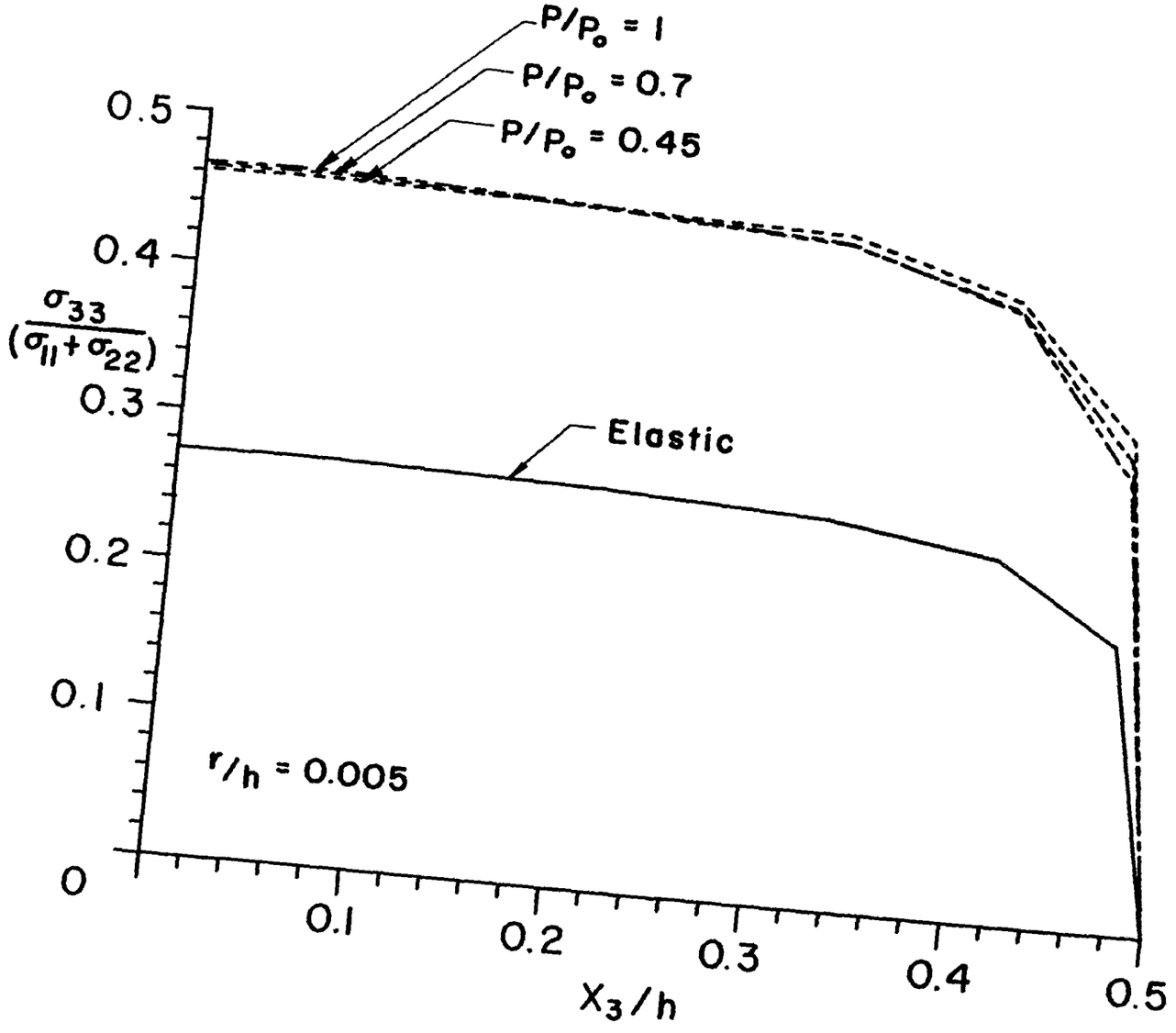

Figure 8.: Variation of the plane strain constraint, $\sigma_{33} / (\sigma_{22} + \sigma_{22})$, along the crack front.

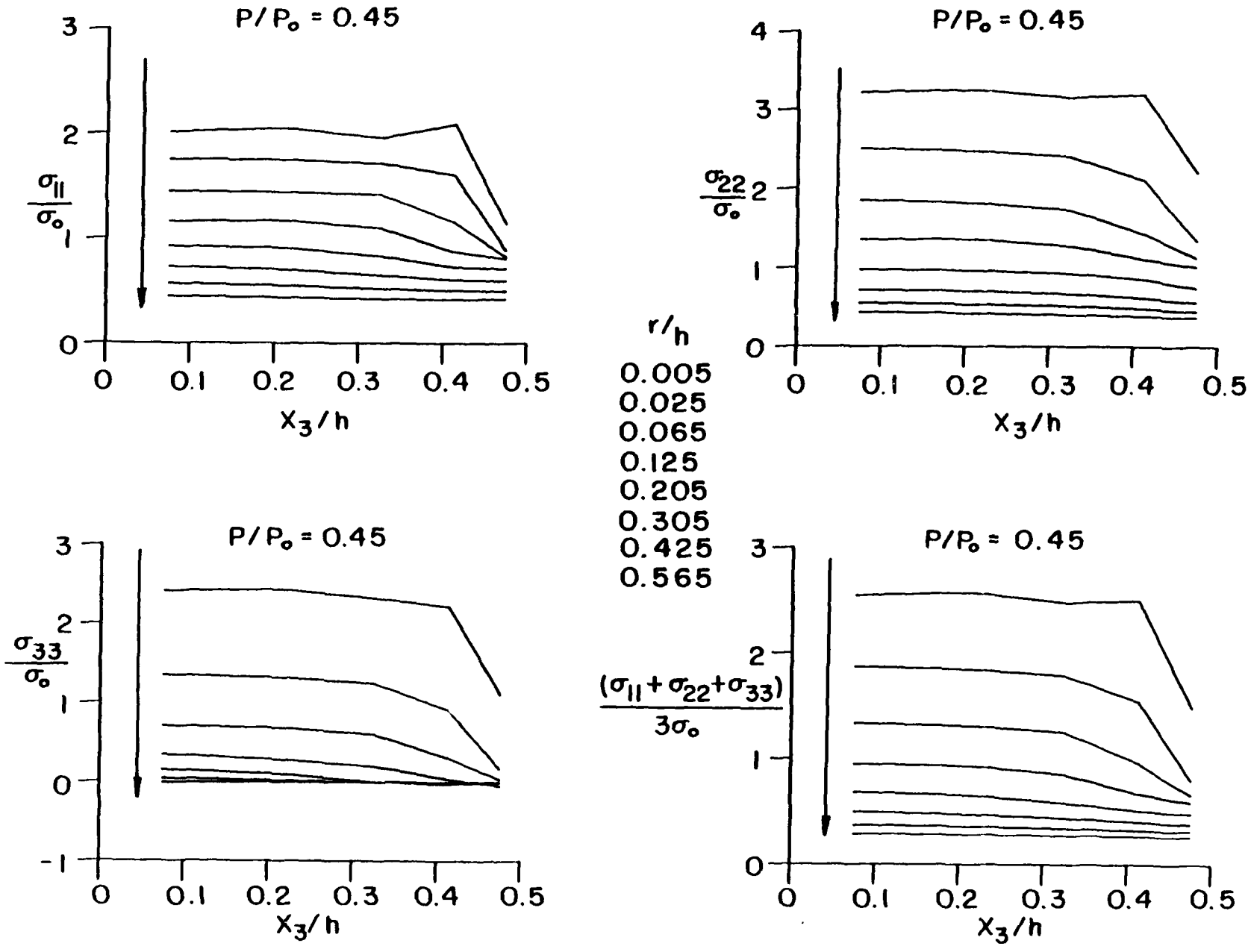

Figure 9.: Variation of normalized stress components through the thickness for load ratio P/P_o = 0.45. The curves shown correspond to r/h - 0.005, 0.025, 0.065, 0.125, 0.205, 0.305, 0.425 and 0.565. The arrow direction indicates increasing r/h values.

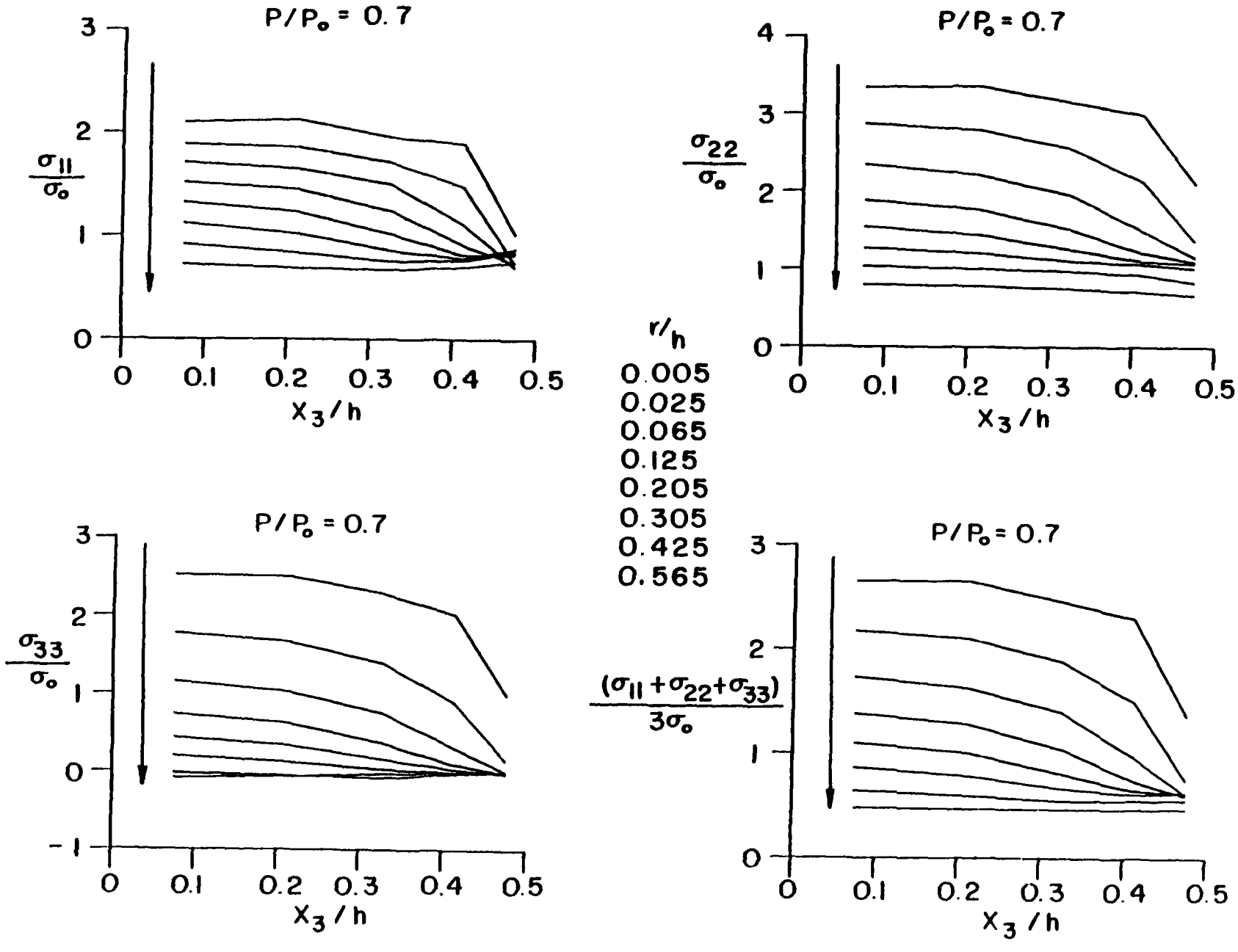

Figure 10.: Variation of normalized stress components through the thickness for load ratio P/P_0 = 0.7. The curves shown correspond to r/h - 0.005, 0.025, 0.065, 0.125, 0.205, 0.305, 0.425 and 0.565. The arrow direction indicates increasing r/h values.

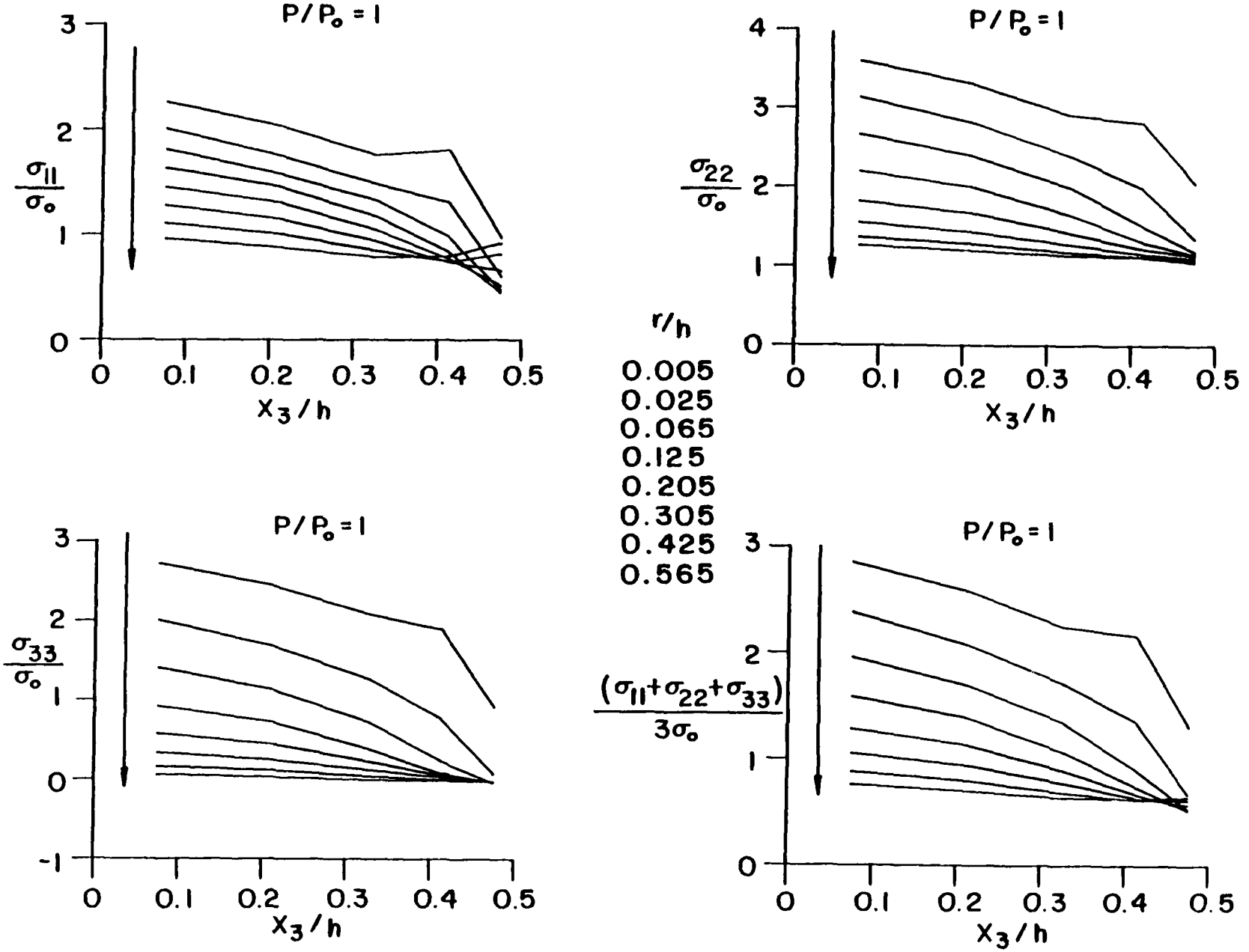

Figure 11.: Variation of normalized stress components through the thickness for load ratio P/P_0 = 1.0. The curves shown correspond to r/h - 0.005, 0.025, 0.065, 0.125, 0.205, 0.305, 0.425 and 0.565. The arrow direction indicates increasing r/h values.

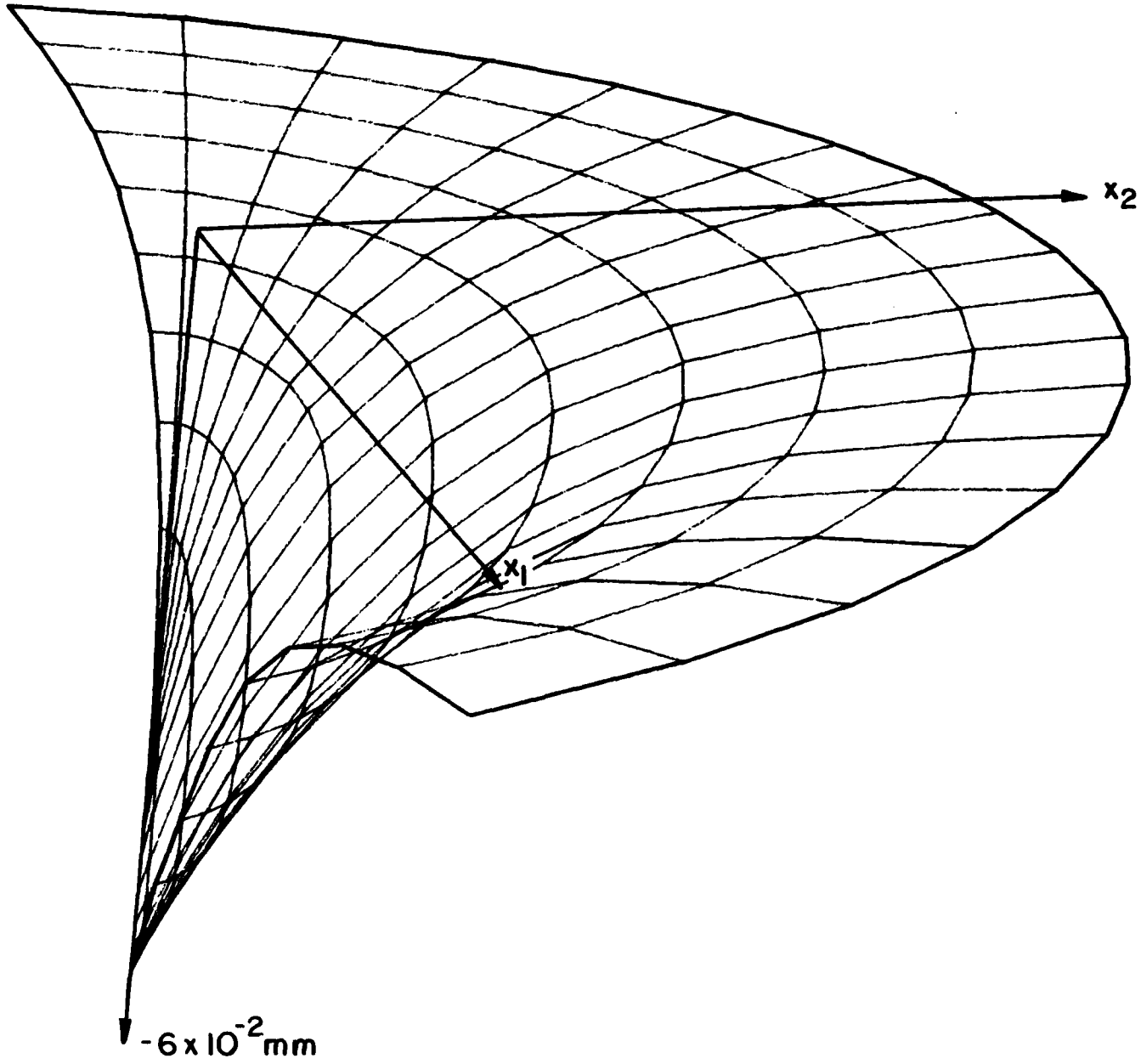

Figure 12a.: Out-of-plane displacement u_3 for load of 52300 N.

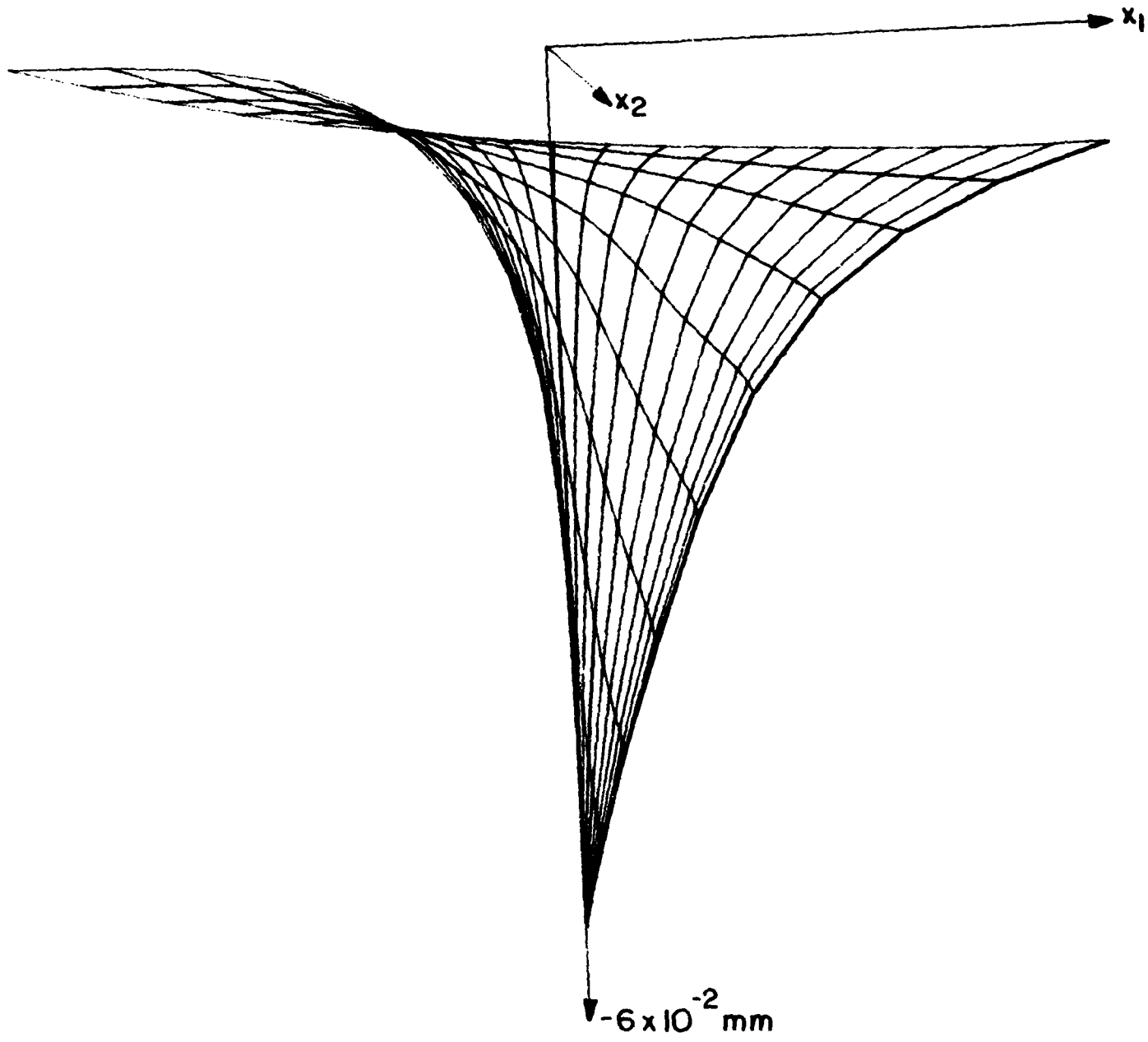

Figure 12b.: Out-of-plane displacement u_3 for load of 52300 N.

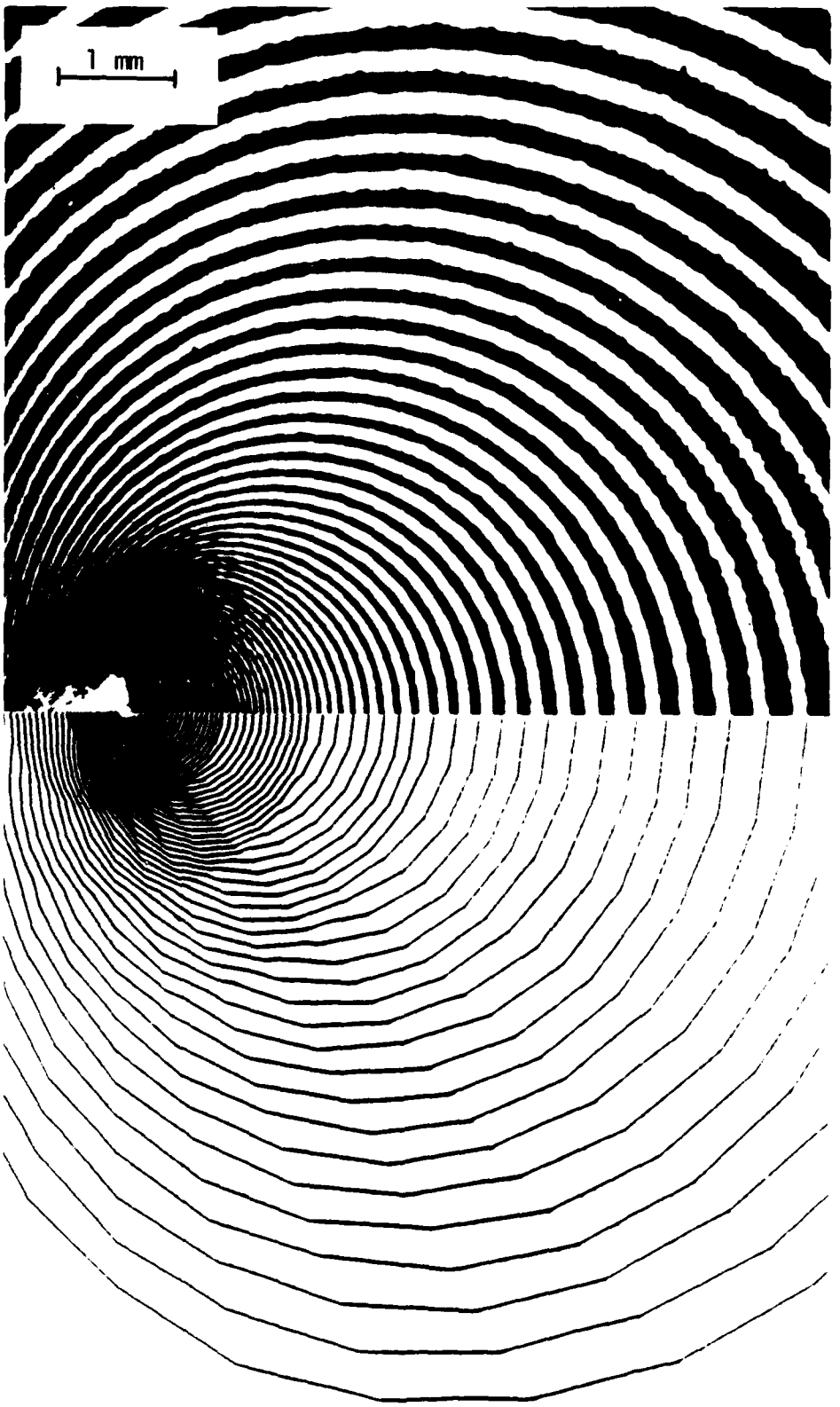

Figure 13.: Comparison of Experimental and Numerical Interferograms, corresponding to the same load level. Fringes are contours of equal out of plane displacement.

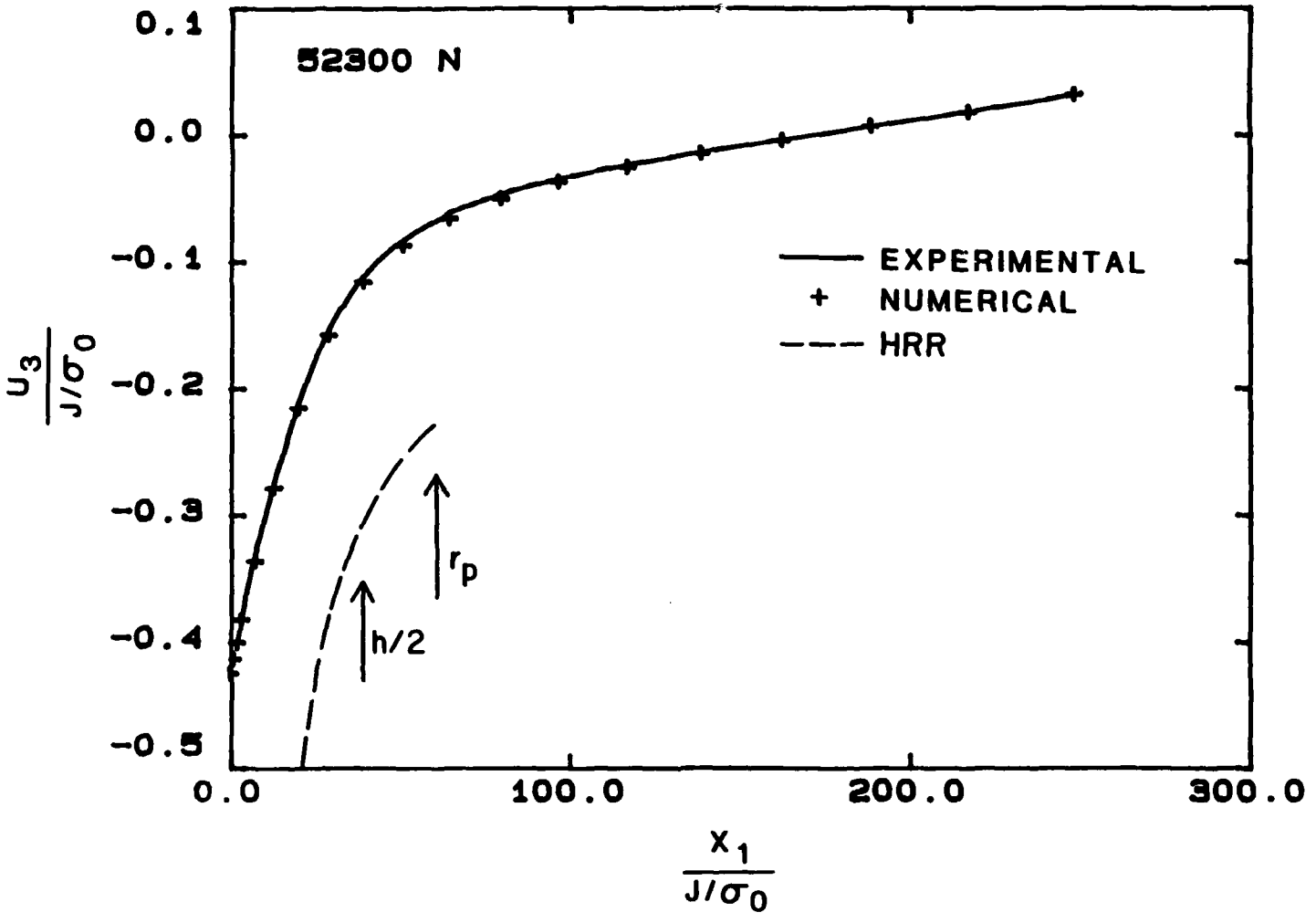

Figure 14.: Nondimensional u_3 displacement on the $\theta = 0$ line. Comparison of experimental and 3-D numerical results for load of 52300 N. Also shown is the HRR field within the plastic zone.

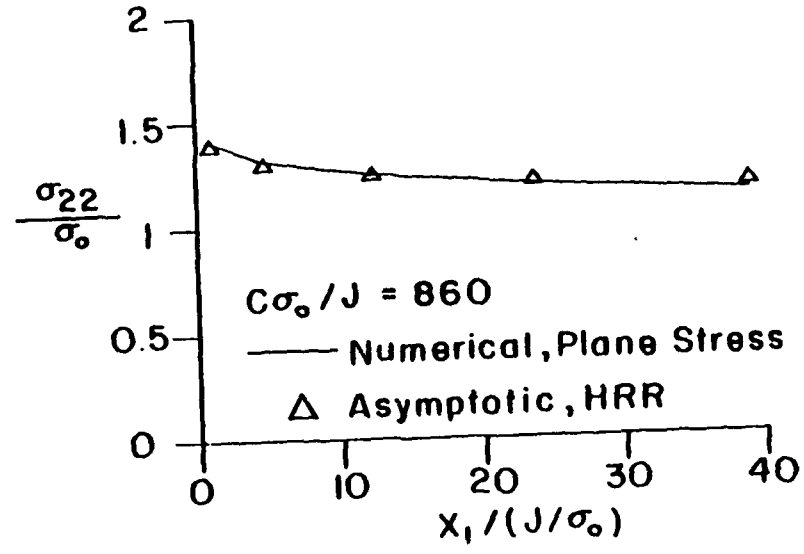

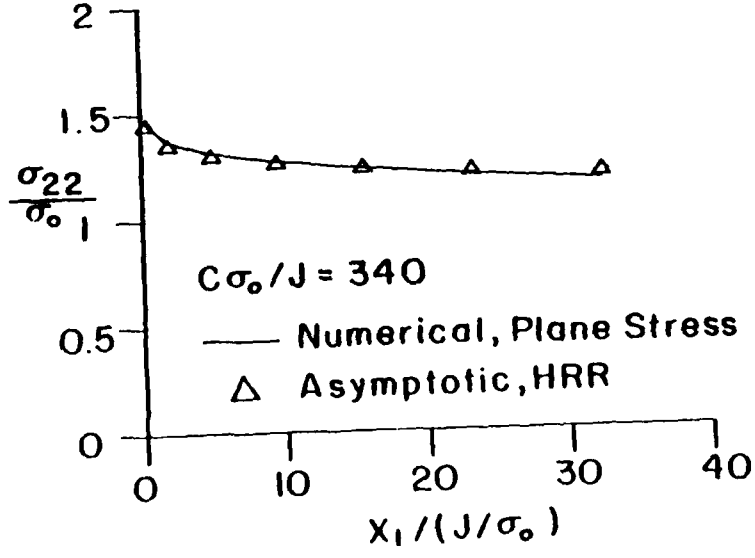

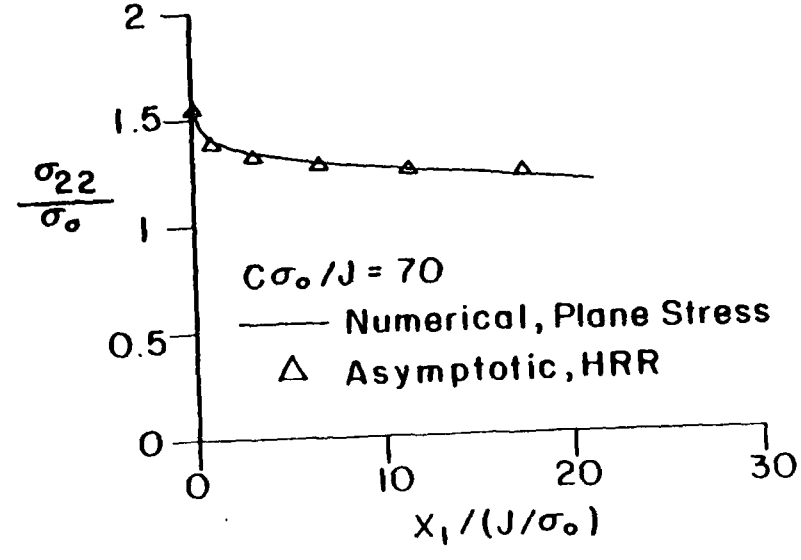

Figure 15.: σ_{22}/σ_o versus normalized distance ahead of the crack tip. Comparison between plane stress numerical and HRR solutions for different extents of yielding from contained to fully plastic conditions.

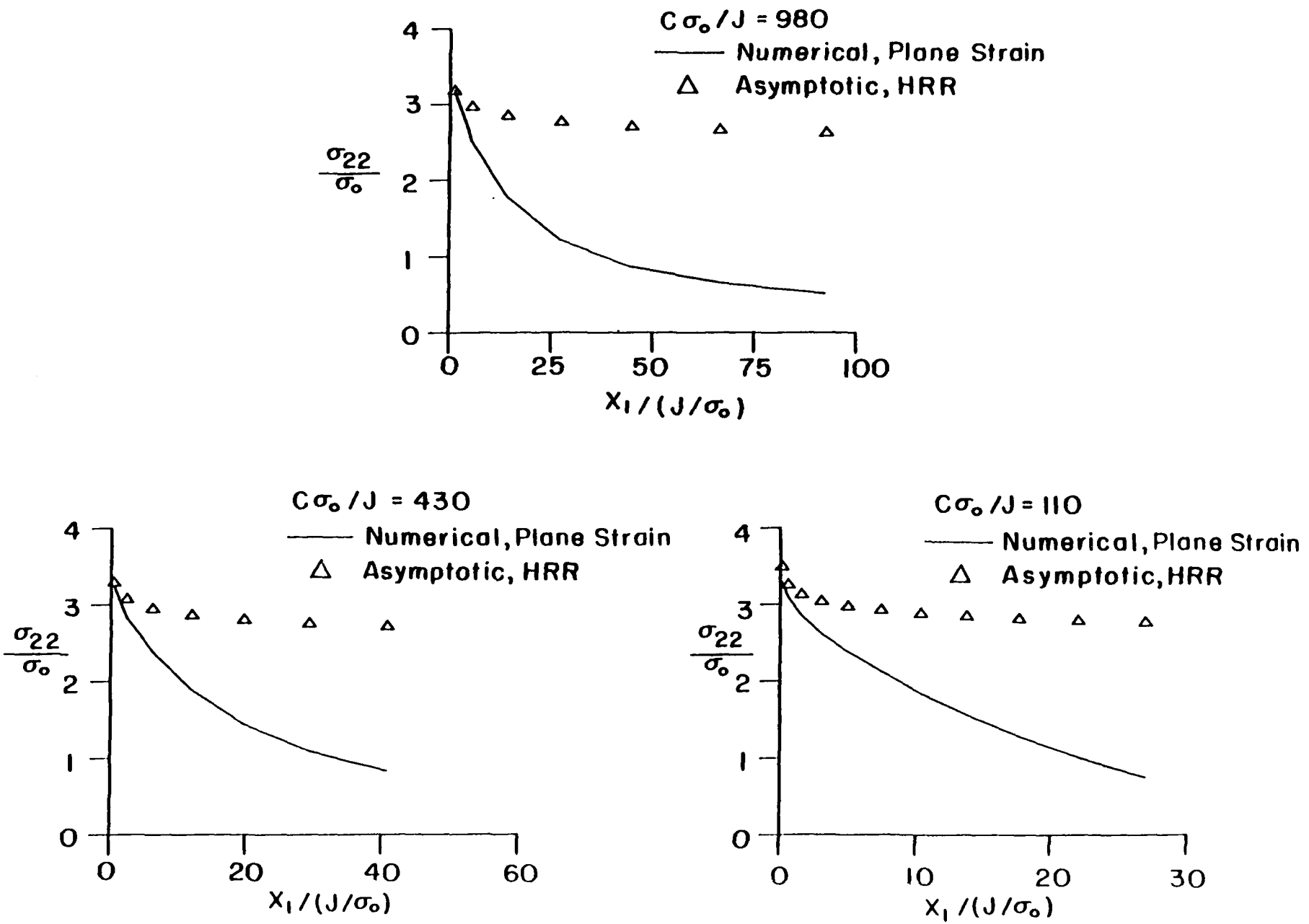

Figure 16.: σ_{22}/σ_o versus normalized distance ahead of the crack tip. Comparison between plane strain numerical and HRR solutions from contained to fully plastic conditions.

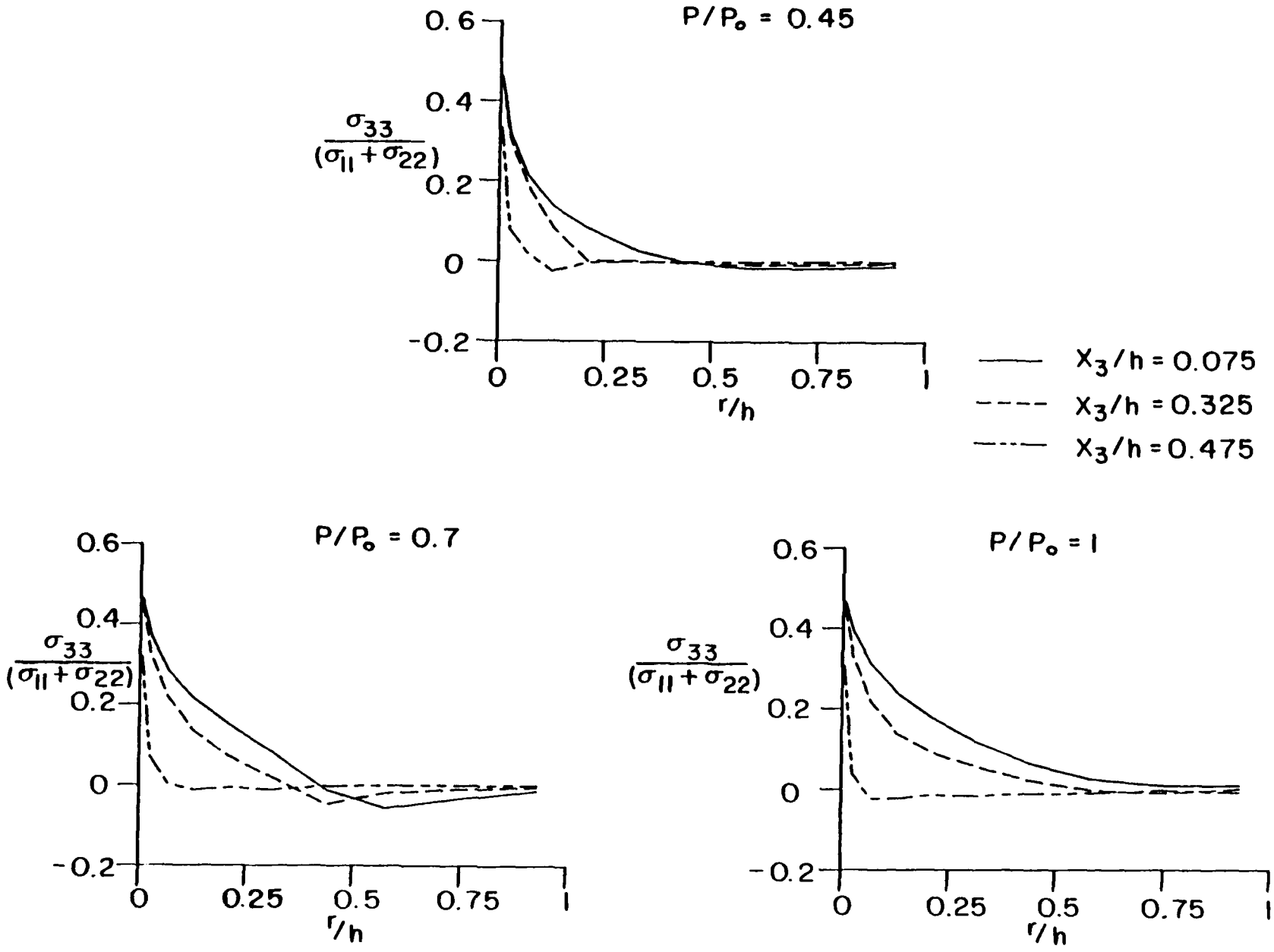

Figure 17.: Radial variation of plane strain constraint $\sigma_{33}/(\sigma_{11} + \sigma_{22})$ along three different planes through the specimen thickness. Results are given for three different load ratios.

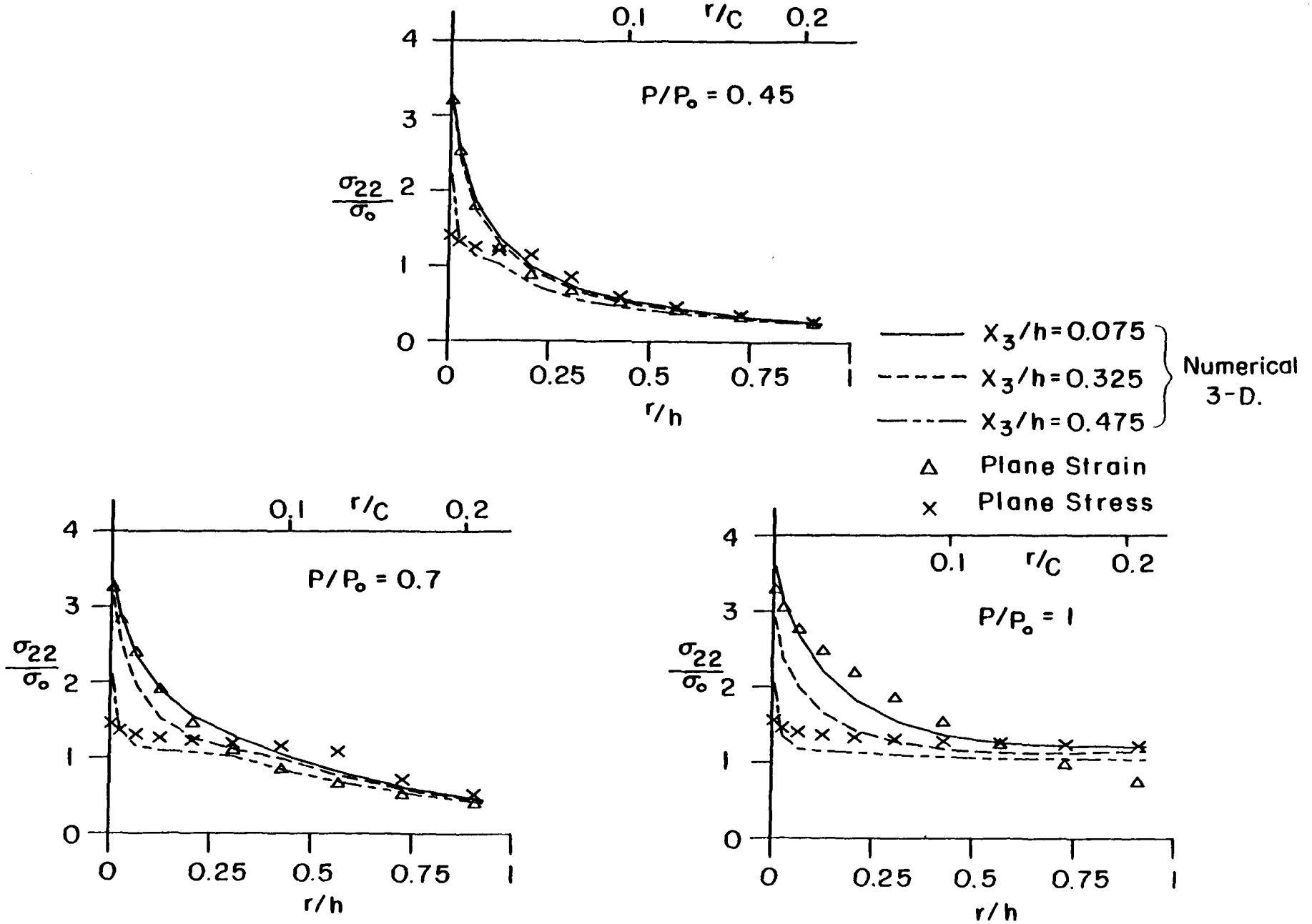

Figure 18.: Radial variation of σ_{22} / σ_o along three different planes through the specimen thickness. Comparison between 3-D, plane strain and plane stress numerical results at the same load levels.

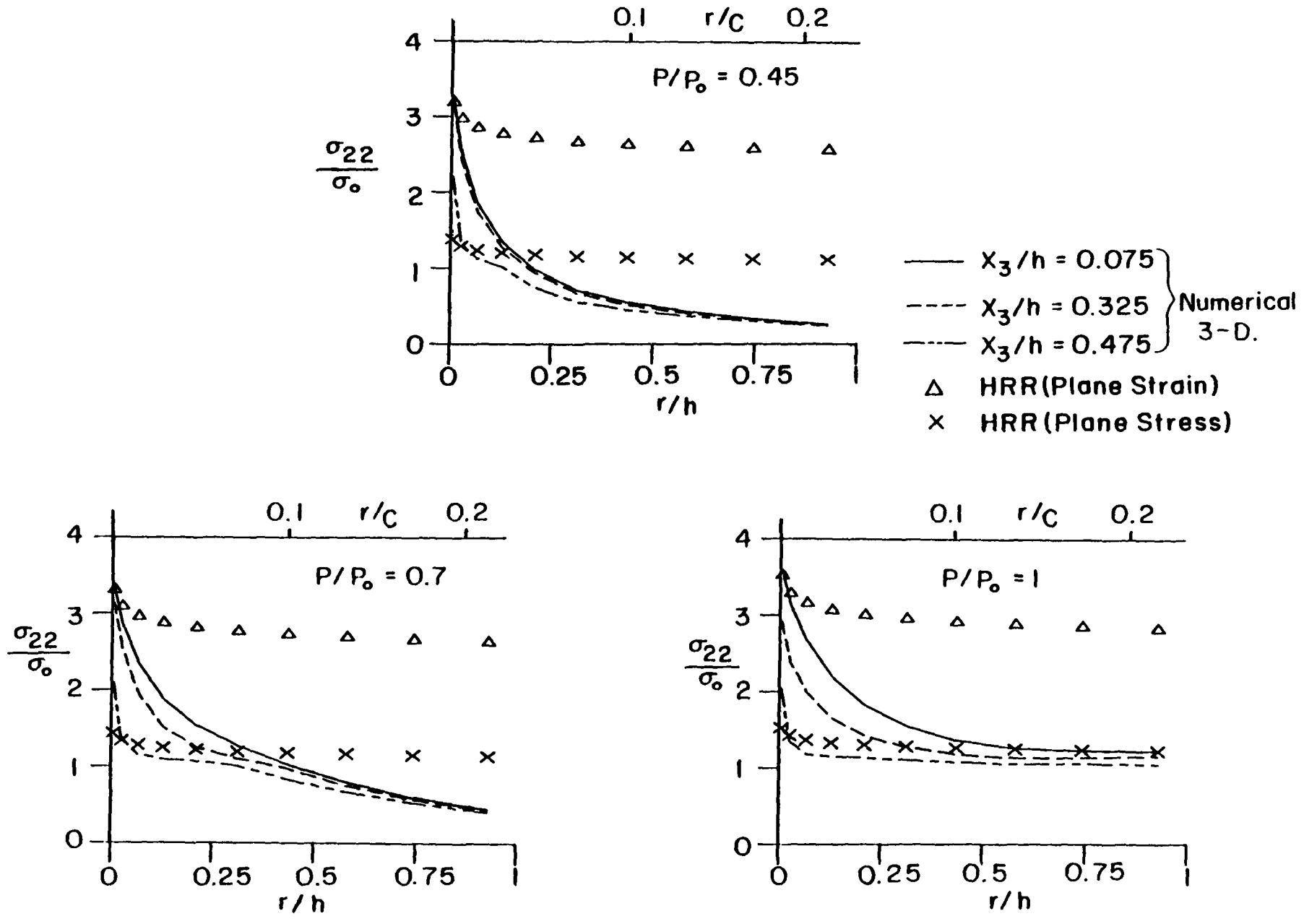

Figure 19.: Radial variation of σ_{22} / σ_o along three different planes through the specimen thickness. Comparison between 3-D numerical and 2-D HRR solutions.

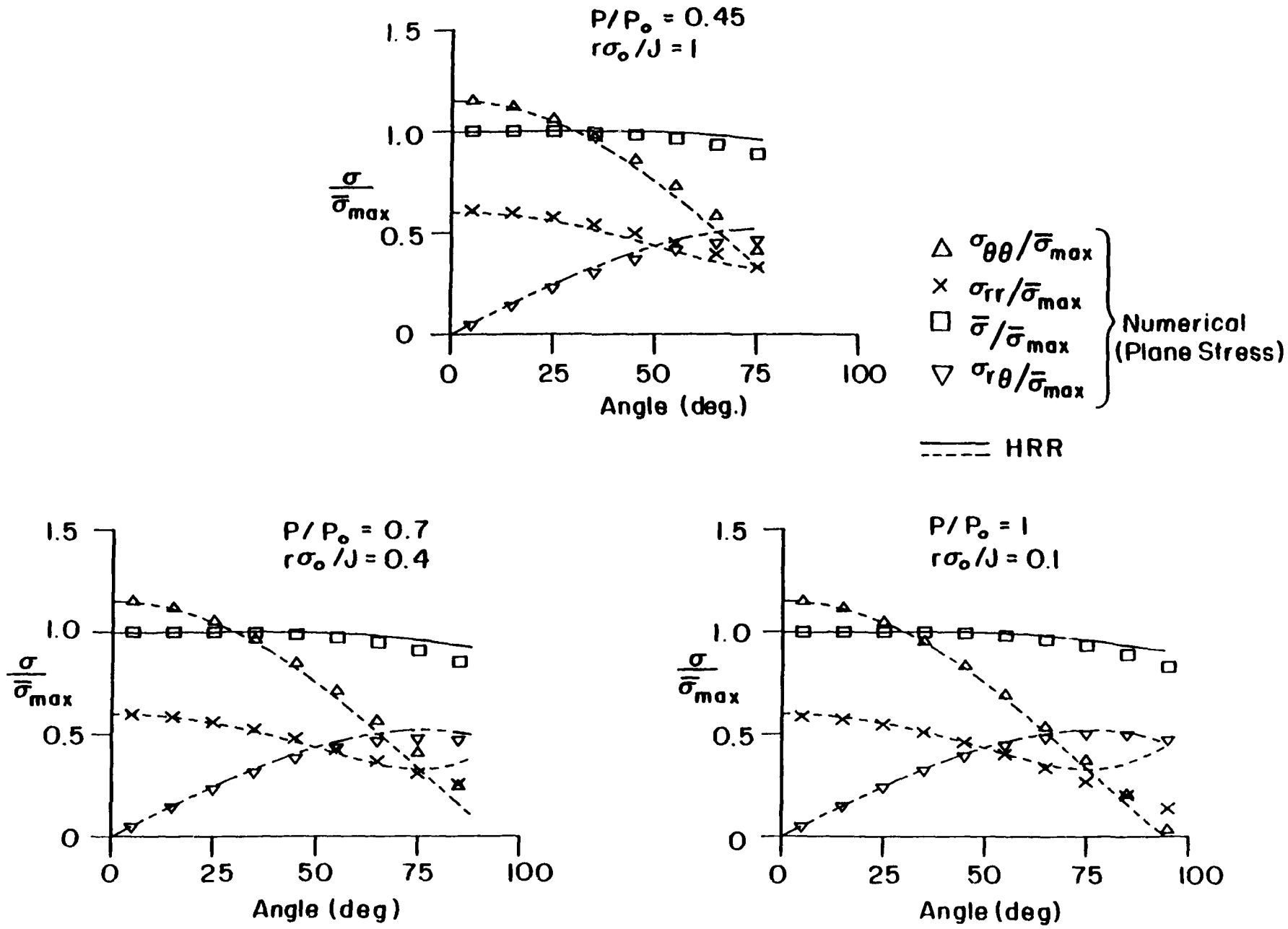

Figure 20.: Near-tip angular stress variation. Comparison between plane stress numerical and HRR solutions from contained to fully plastic conditions.

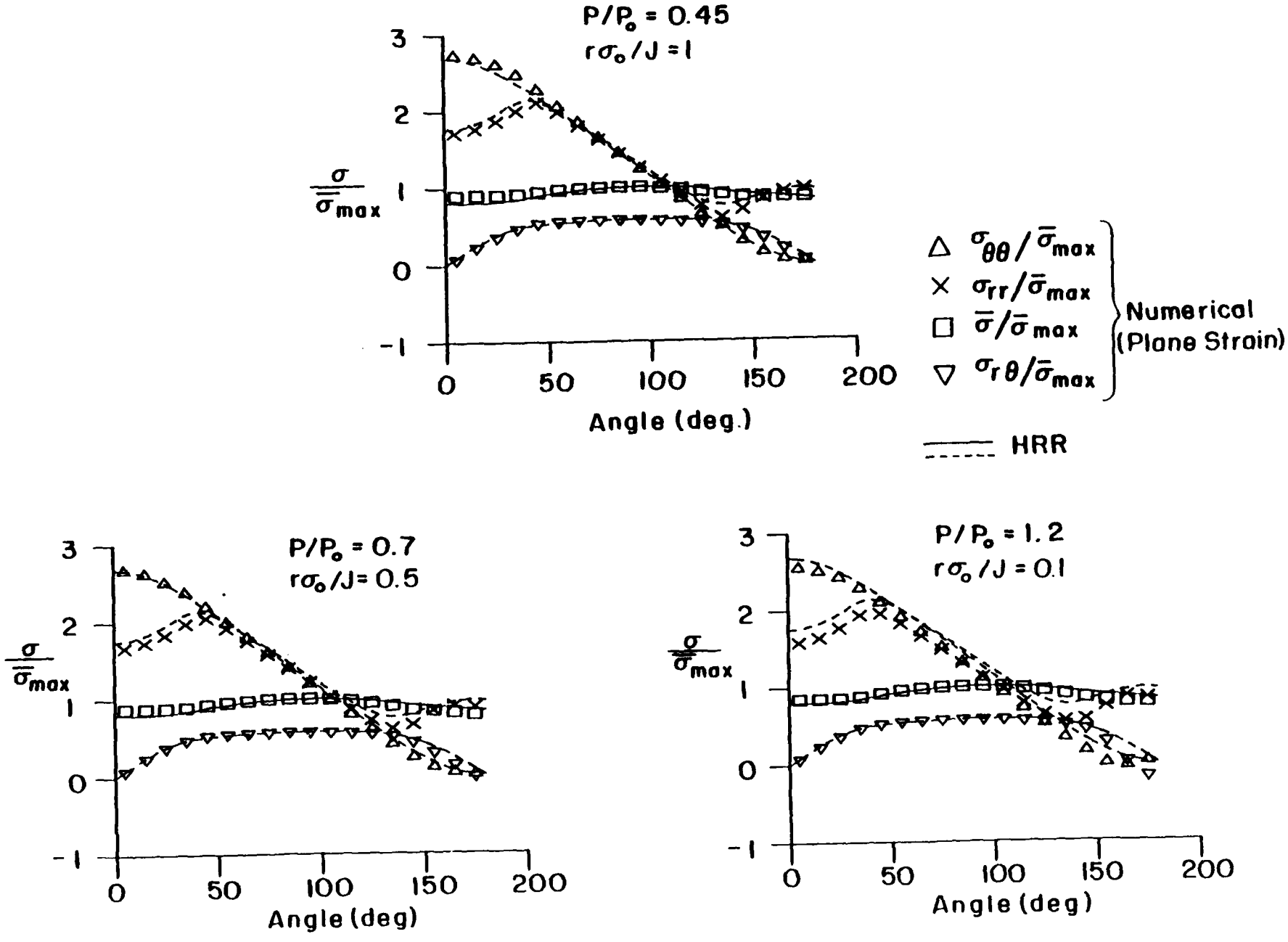

Figure 21.: Near-tip angular stress variation. Comparison between plane strain numerical and HRR solutions from contained to fully plastic conditions.

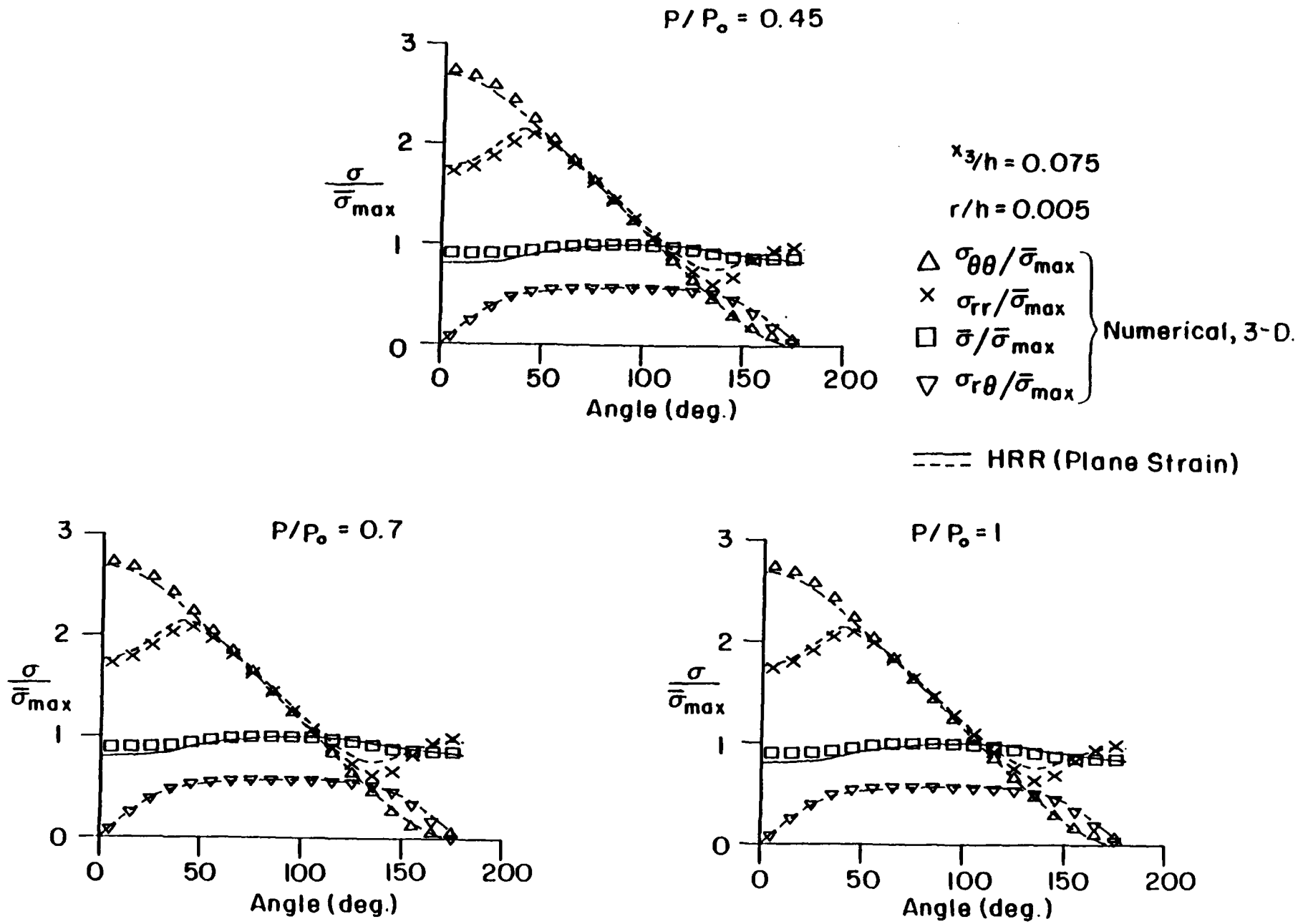

Figure 22.: Comparison between 3-D near-tip angular stress distribution along the plane $x_3 / h = 0.075$ and HRR plane strain solution.

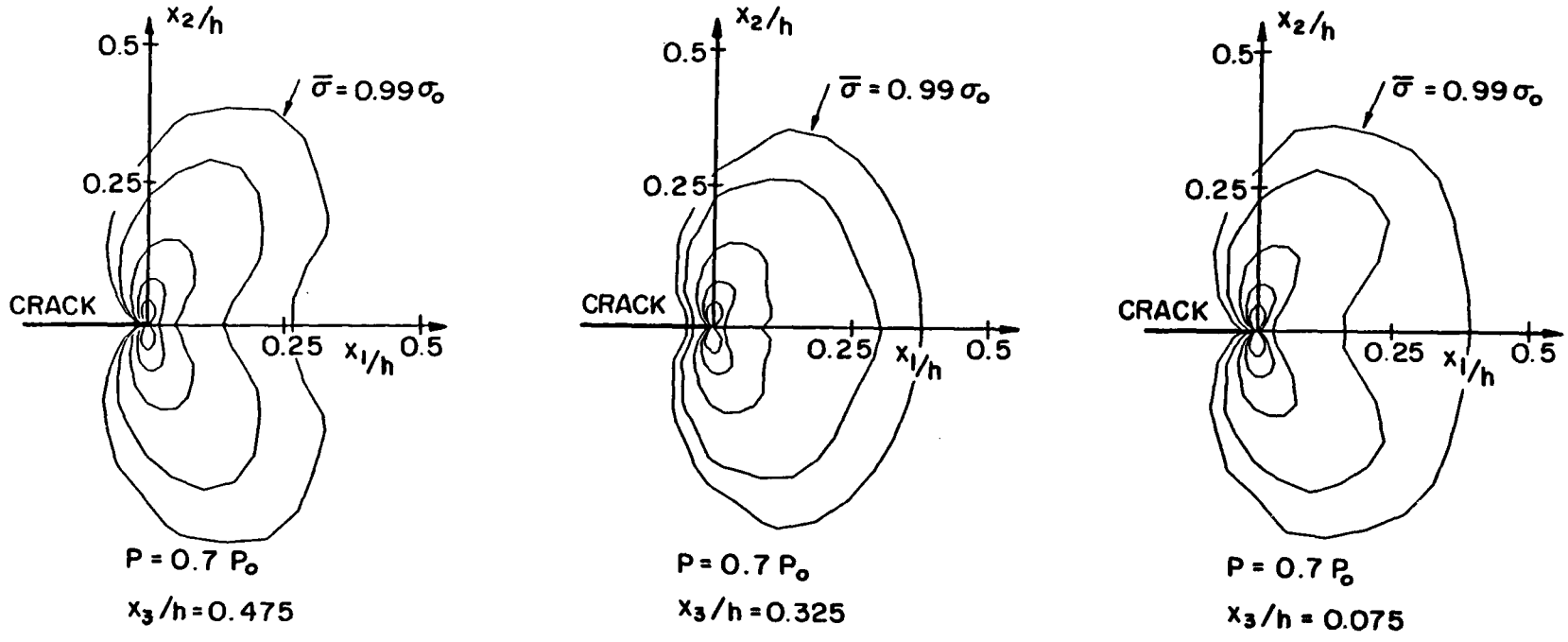

Figure 23.: Contours of equivalent stress ($\bar{\sigma} / \sigma_o$ = 0.99, 1.02, 1.05, 1.08, 1.11) for P/P_0 = 0.7 at x_3 / h = 0.075, 0.325, 0.475.

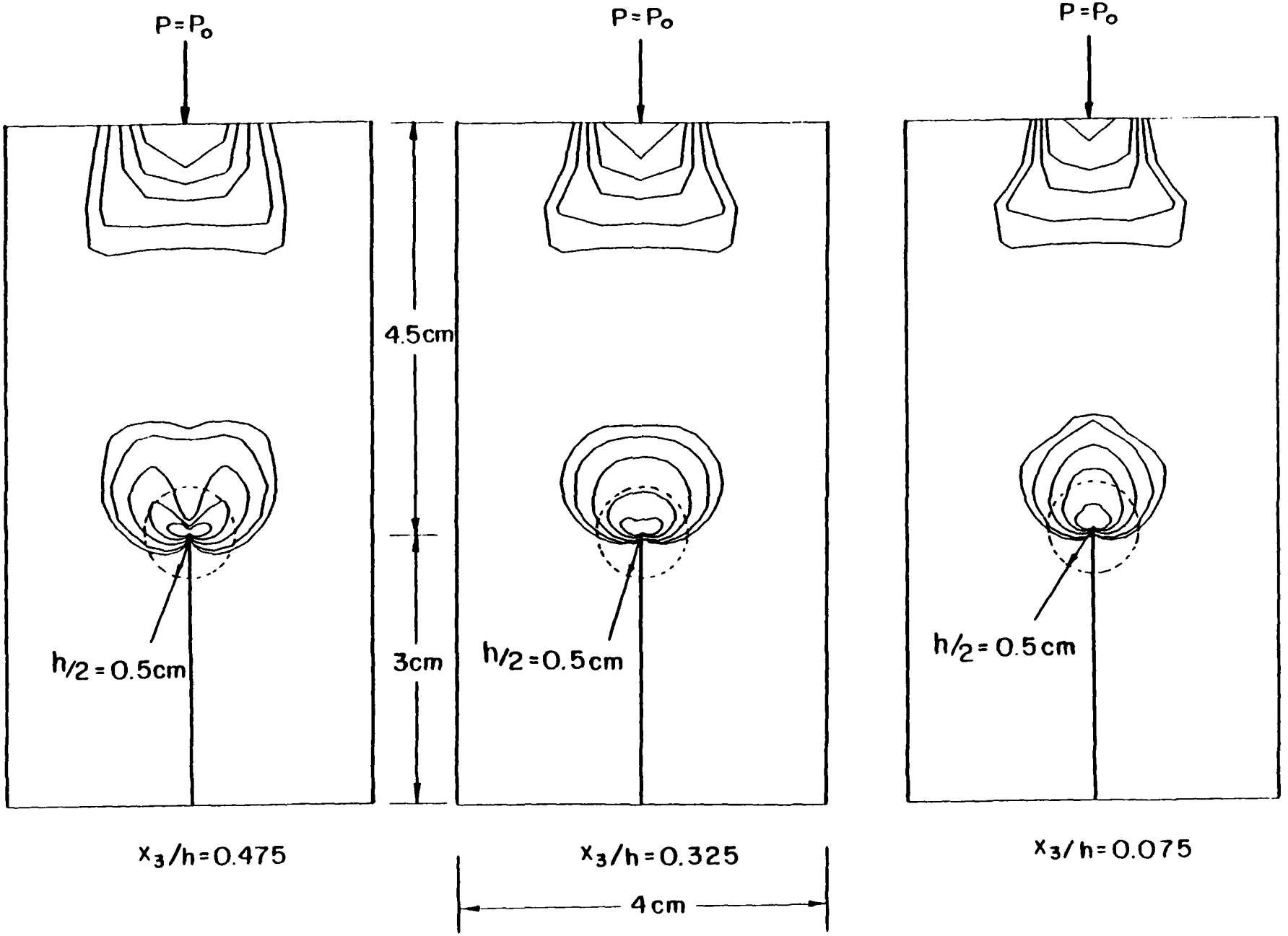

Figure 24.: Contours of equivalent stress ($\bar{\sigma} / \sigma_o$ = 0.99, 1.02, 4.05, 1.08, 1.11) for $P/P_0 = 1$ at $x_3 / h = 0.075, 0.325, 0.475$.

SECURITY CLASSIFICATION OF THIS PAGE (When Data Entered)

REPORT DOCUMENTATION PAGE		READ INSTRUCTIONS BEFORE COMPLETING FORM
1. REPORT NUMBER SM 88-6	2. GOVT ACCESSION NO.	3. RECIPIENT'S CATALOG NUMBER
4. TITLE (and Subtitle) Three Dimensional Effects Near a Crack Tip in a Ductile Three Point Bend Specimen Part I:Numerical Analysis		5. TYPE OF REPORT & PERIOD COVERED 6. PERFORMING ORG. REPORT NUMBER
7. AUTHOR(s) R. Narasimhan and A.J. Rosakis		8. CONTRACT OR GRANT NUMBER(s) ONR Contract N00014-85-K-0596
9. PERFORMING ORGANIZATION NAME AND ADDRESS Graduate Aeronautical Laboratories, 105-50 California Institute of Technology Pasadena, CA 91125		10. PROGRAM ELEMENT, PROJECT, TASK AREA & WORK UNIT NUMBERS
11. CONTROLLING OFFICE NAME AND ADDRESS Dr. Yapa Rajapakse, Program Manager ONR, Code 1132SM 800 N. Quincy St., Arlington, VA 22217-5000		12. REPORT DATE January 1988 13. NUMBER OF PAGES 21
14. MONITORING AGENCY NAME & ADDRESS(if different from Controlling Office)		15. SECURITY CLASS. (of this report) unclassified 15a. DECLASSIFICATION/DOWNGRADING SCHEDULE

16. DISTRIBUTION STATEMENT (of this Report)

17. DISTRIBUTION STATEMENT (of the abstract entered in Block 20, if different from Report)

18. SUPPLEMENTARY NOTES

Submitted for publication in Journal of Applied Mechanics.

19. KEY WORDS (Continue on reverse side if necessary and identify by block number)

Elastic- Plastic fracture, three dimensions, finite elements

20. ABSTRACT (Continue on reverse side if necessary and identify by block number)

A simultaneous numerical and experimental investigation is undertaken to assess three dimensional effects and HRR dominance near a crack front in a ductile 3-point bend specimen. In parallel to the 3-D numerical calculations, a plane-strain and a plane-stress analysis of the same in-plane specimen geometry is performed to obtain upper and lower bounds for the 3-D calculation. The radial, angular and thickness variation of the stresses and displacements are studied in great detail from contained yielding, to fully plastic conditions. The results indicate that the

DD FORM 1 JAN 73 1473 EDITION OF 1 NOV 65 IS OBSOLETE

S/N 0102-LF-014-6601

SECURITY CLASSIFICATION OF THIS PAGE (When Data Entered)

plane strain HRR field prevails in the interior of the specimen very near the crack front even for moderate extents of yielding. On the other hand, for distances from the crack tip exceeding about half a specimen thickness, plane stress conditions are approached.

The calculations presented here model a series of laboratory experiments involving three independent experimental techniques. Details regarding the experiments and comparisons of the experimental measurements with numerical calculations and theory are emphasized in Part II of this work.